The Receptor Recycling Pathway Contains Two Distinct Populations of Early Endosomes with Different Sorting Functions

David R. Sheff, Elizabeth A. Daro, Michael Hull, and Ira Mellman

Department of Cell Biology, Yale University School of Medicine, New Haven, Connecticut 06520-8002

Abstract. Receptor recycling involves two endosome populations, peripheral early endosomes and perinuclear recycling endosomes. In polarized epithelial cells, either or both populations must be able to sort apical from basolateral proteins, returning each to its appropriate plasma membrane domain. However, neither the roles of early versus recycling endosomes in polarity nor their relationship to each other has been quantitatively evaluated. Using a combined morphological, biochemical, and kinetic approach, we found these two endosome populations to represent physically and functionally distinct compartments. Early and recycling endosomes were resolved on Optiprep gradients and shown to be differentially associated with rab4, rab11, and transferrin receptor; rab4 was enriched on early endosomes and at least partially depleted from recycling endosomes, with the opposite being true for rab11 and transferrin receptor. The two populations were also pharmacologically distinct, with AlF_4 selectively blocking export of transferrin receptor from recycling endosomes to the basolateral plasma membrane. We applied these observations to a detailed kinetic analysis of transferrin and dimeric IgA recycling and transcytosis. The data from these experiments permitted the construction of a testable, mathematical model which enabled a dissection of the roles of early and recycling endosomes in polarized receptor transport. Contrary to expectations, the majority (>65%) of recycling to the basolateral surface is likely to occur from early endosomes, but with relatively little sorting of apical from basolateral proteins. Instead, more complete segregation of basolateral receptors from receptors intended for transcytosis occurred upon delivery to recycling endosomes.

Key words: sorting • endosomes • receptor recycling

EPITHELIAL cells maintain polarity due in part to the ability of endosomes to return receptors, proteins, and lipids internalized by endocytosis to their correct plasma membrane domains (Mellman, 1996). For example, in MDCK cells receptors for transferrin (Tfn)[1] and low density lipoprotein remain enriched at the basolateral plasma membrane because they are selectively packaged into recycling vesicles targeted to their site of origin. Conversely, the polymeric immunoglobulin receptor (pIgR) can mediate the transcytosis of basolaterally internalized dimeric IgA (dIgA) due to the ability of endosomes to sort IgA–pIgR complexes into vesicles targeted to the apical surface (Breitfeld et al., 1989; Apodaca et al., 1994; Gibson et al., 1998).

In MDCK cells, polarized targeting in endosomes appears to rely on much the same sorting signals that control the polarized targeting on the secretory pathway, at the level of the trans-Golgi network (Matter et al., 1993). The cytoplasmic domains of most basolateral proteins contain one or more distinctive signals that specify their transport to the basolateral domain (Trowbridge et al., 1984; Matter et al., 1992, 1993; Matter and Mellman, 1994; Mostov, 1995; Lai et al., 1998). Often, these signals contain critical tyrosine or di-leucine motifs and therefore may be decoded by a mechanism related to clathrin adaptor complexes (Futter et al., 1998). Apical targeting occurs in the absence of a functional basolateral signal, and can be rendered more efficient by the recognition of lumenal carbohydrate residues or possibly transmembrane anchor features. Apical targeting may involve sequestration into glycosphingolipid-enriched "rafts" (Simons and Ikonen, 1997).

Determining where in the endocytic pathway apical and basolateral proteins are sorted has remained difficult, in

Elizabeth A. Daro's current address is Immunex, 51 University St., Seattle, WA 98101.

Address correspondence to Ira Mellman, Dept. of Cell Biology, Yale University School of Medicine, 333 Cedar St., P.O. Box 208002, New Haven, CT 06520-8002. Tel.: (203) 785-4303 or 4302. Fax: (203) 785-4301. E-mail: ira.mellman@yale.edu

1. *Abbreviations used in this paper:* dIgA, dimeric IgA; EE, early endosome; LE, late endosome; pIgR, polymeric immunoglobulin receptor; RE, recycling endosome; Tfn, transferrin.

part due to the inability to resolve endosome populations into their component parts. There are at least three potential endosomal compartments in polarized and nonpolarized cells (Mellman, 1996). Early endosomes (EEs) in the peripheral cytoplasm are defined as the first to receive cargo from incoming clathrin-coated vesicles. Due to their acidic internal pH, EEs facilitate the dissociation of many receptor–ligand complexes. Dissociated ligands and other fluid phase components are then delivered to late endosomes (LEs) while the receptors are sorted into recycling vesicles destined for the plasma membrane. Interestingly, recycling receptors appear to accumulate in a population of vesicles, generally termed recycling endosomes (REs), which in many cell types are concentrated at the microtubule organizing center (Apodaca et al., 1994; Daro et al., 1996). Although direct evidence is lacking, REs are thought to represent an obligatory intermediate on the recycling pathway (Presley et al., 1993; Apodaca et al., 1994; Barroso and Sztul, 1994; Ghosh and Maxfield, 1995; Lauffenburger and French, 1996). However, there is increasing reason to believe that REs comprise a population of endosomes distinct from EEs. REs are devoid of fluid markers, suggesting that they do not have a role in receptor-ligand sorting. Moreover, fluorescence microscopy has indicated that REs are enriched in rab11 and depleted in rab4, whereas EEs have the opposite phenotype; there may also be differences in t-SNARE composition (Ullrich et al., 1996; Advani et al., 1998). REs may also be capable of sorting polyvalent from monomeric TfnR (Marsh et al., 1995).

In polarized MDCK cells, REs appear to localize in the apical cytoplasm and are often referred to as apical endosomes (Apodaca et al., 1994). Their possible role as a distinct sorting site for polarized recycling is suggested by the observation that one or more populations of these apical endosomes can be accessed by ligands that recycle basolaterally (Tfn), ligands engaged in basolateral to apical transcytosis (dIgA), as well as markers that recycle at the apical surface (Apodaca et al., 1994; Gibson et al., 1998). However, neither their actual identity nor role in sorting has been directly or quantitatively evaluated. Apical endosomes may only be involved in sorting only that fraction of basolateral markers which were missorted in peripheral EEs. Alternatively, they may not be involved in sorting at all. Since a fraction of Tfn internalized basolaterally is normally missorted to the apical surface (Odorizzi et al., 1996), Tfn found in apical REs may represent apically destined ligand. Finally, EM cytochemical analysis has suggested that all endosomes in polarized cells form a single continuous tubulovesicular network (Odorizzi et al., 1996). In this case, movement between the elements of the network would be a diffusion-limited process and separate compartments and sorting sites would not exist.

In both polarized and nonpolarized cells, the kinetics of Tfn recycling consist of distinct fast ($t_{1/2}$ = 5 min) and slow ($t_{1/2}$ = 15–30 min) components (Hopkins and Trowbridge, 1983; Mayor et al., 1993; Presley et al., 1993; Hopkins, 1994; Gruenberg and Maxfield, 1995). The significance of these complex kinetics is not clear, and may reflect any of a variety of possibilities ranging from the ability of REs to partially retain recycling receptors to the existence of multiple pathways through the recycling network. We now provide direct evidence that MDCK cells contain biochemically distinct EE and RE compartments which play functionally distinct roles in receptor recycling.

Materials and Methods

Biochemical Reagents

All reagents were of analytical grade or higher and were purchased from Sigma Chemical Co. unless otherwise noted. FITC-Tfn was purchased from Molecular Probes Inc. ^{125}I was purchased from Amersham. Human holo-Tfn was purchased from Sigma Chemical Co. Human dIgA was a kind gift from J.P. Vaerman and Yves Sibille (Brussels, Belgium). Tfn and dIgA were radioiodinated using Iodogen to specific activities of ~5 μCi/μg.

Density Gradient Separation of Endosomal Compartments

MDCK cells transfected with human Tfn receptor (in pCB6 maintained with G418 selection) and rabbit pIgR (in pCEP4 maintained with hygromycin selection) were grown in DMEM plus 10% FCS. Cells were split 1:10 every 5–7 d. Confluent cells from a T-75 culture flask were trypsinized and plated into 2 × 75 mm Transwell cell culture inserts (Costar/Corning). After 3 d, the cells were induced with 10 mM butyrate for 16 h. Cells were then kept in serum-free media at 37°C for 30 min before transfer into ice cold PBS^{2+} (PBS with 0.9 mM $CaCl_2$, 0.5 mM $MgCl_2$). Inserts were removed and placed onto 250 μl of 10 μg/ml labeled Tfn or dIgA in 1.5% (wt/vol) BSA for 1 h on ice. Cells were then washed five times for 5 min each in ice-cold PBS^{2+}. Transwells were then placed in empty culture dishes in a 37°C water bath. Warm DMEM containing 100 μg/ml unlabeled holo-Tfn was added to the upper and lower chambers. Transwell units were removed to ice-cold PBS^{2+} after 2.5, 20, or 25 min. Surface bound Tfn was removed with two successive 5-min washes in acid citrate (25 mM citric acid, 24.5 mM Na citrate, 280 mM sucrose, pH 4.6) and PBS^{2+}. For dIgA, surface bound ligand was stripped with washes of DMEM plus 10 mM phosphate brought to pH 2.95. Cells were then scraped with a rubber policeman into 1 ml ICT (78 mM KCl, 4 mM $MgCl_2$, 8.37 mM $CaCl_2$, 10 mM EGTA, 50 mM Hepes/KOH, pH 7.0) plus 250 mM sucrose, and passed four times through a ball bearing homogenizer using a 0.2496 inch ball bearing. A PNS was generated by centrifugation at 1,000 *g* for 5 min. The PNS was placed on a 5–20% (10–20% for immunoblots) linear Optiprep (Nycomed) gradient formed in ICT using a Gradient Master (Biocomp). Gradients were spun in an SW41 ultracentrifuge head (Beckman) for 18–20 h at 27,000 rpm (100,000 *g* at the tube bottom) at 4°C. Gradients were harvested using an auto Densi-Flow gradient harvester (Buchler). Gradient linearity was checked by refractive index. The plasma membrane was localized by alkaline phosphodiesterase activity (Green et al., 1987).

Fluorescent Labeling of Endosomes

For single cohort internalization studies, MDCK cells transfected as above were sown at confluence on clear Transwell filters (0.4 μm pore) and incubated 3 d to polarize. Cells were induced with 10 mM butyrate overnight. Cells were incubated in serum-free media for 45 min to deplete Tfn. FITC-Tfn and/or Texas red–dIgA (produced from dIgA above using Texas red labeling kit from Molecular Probes) was bound to the basolateral surface at 0°C for 1 h. The cells were washed for 5 min, five times with PBS supplemented with ice-cold PBS^{2+} as above. Ligands were internalized for either 2.5 or 25 min in DMEM media containing 100 μg/ml unlabeled Tfn and 10 mM Hepes. The cells were fixed in 3% PFA in PBS and then mounted in Moviol (Calbiochem) containing DABCO (Sigma Chemical Co.). Images were acquired with an excitation wavelength of 495 nm and an emission wavelength of 520 nm with either a 100× or 63× objective using a Axioplan microscope (Carl Zeiss) equipped with a digital camera (Princeton Instruments). The microscope and camera were driven by Openlab 1.7.6 (Improvision) run on an Apple Macintosh 9600.

For preloaded cells and chase studies, MDCK cells transfected as above or CHO cells transfected with the human TfnR (in pCB6 maintained with G418 selection) were grown on 1-oz coverslips in DMEM (MDCK) or aMEM (CHO). Cells were sown thinly and induced while subconfluent using butyrate for 12–16 h. Cells were preincubated in serum-free media for 30 min at 37°C to deplete Tfn. Coverslips were then inverted onto droplets of 100 μg/ml FITC Tfn in serum-free media and in-

cubated at 37°C for 30 min. Label was chased out of the cells with 100 μg/ml unlabeled holo-Tfn in the presence or absence of AlF_4 (50 μM $AlCl_2$, 30 mM NaF) for up to 30 min. Cells were fixed in 3% PFA in PBS and then mounted in Moviol (Calbiochem) containing DABCO (Sigma Chemical Co.). Images were acquired with an excitation wavelength of 495 nm and an emission wavelength of 520 nm using an Axiophot microscope with a 63× objective and 100 ASA Ectachrome film (Kodak). Confocal images were acquired on a Bio-Rad 1050 confocal microscope with an excitation wavelength of 495 nm and an emission wavelength of 520 nm and digitally processed. Images were enhanced and combined using Adobe Photoshop on a Macintosh computer.

Western Blot

Fractions from Optiprep density gradients were mixed with an equal volume of H_2O containing 2% (wt/vol) sodium deoxycholate (Sigma Chemical Co.) and vortexed. Each fraction was brought to 10% trichloroacetic acid (Brand Nu Laboratories). After 30 min on ice, the precipitate was collected by centrifugation and the pellets washed for 30 min in two changes of 80% acetone (vol/vol in H_2O). The resulting pellets were dissolved in SDS sample buffer and analyzed by SDS-PAGE followed by Western blot using ECL (Pierce Chemical Co.) detection. Cells from approximately half of a 75-mm Transwell were used for each set of blots. Rab4, cellubrevin, and TfnR antibodies have been described previously (Daro et al., 1996) and Rab11 antibody was purchased from Zymed.

Electron Microscopy

Fractions from Optiprep gradients were directly fixed in Optiprep with 3% paraformaldehyde overnight at 4°C. Vesicles were adhered to grids by floating carbon-coated formvar-nickel EM grids on fixed fractions for 10 min. The grids were then blocked with 1% (wt/vol) fish skin gelatin and washed in PBS. 0.4% uranyl acetate/1.8% methyl cellulose (Sigma Chemical Co.) was then applied for contrast. First primary antibodies (same as for Western blots) were applied at 1:10 dilution in PBS/1% BSA, and a bridging antibody used for the polyclonal anti-rab4 antibody. 5-nm gold labeled secondary antibody was then applied (H. Geuze). The grids were washed and further fixed with glutaraldehyde. The process was then repeated with a second set of primary antibodies and 10-nm gold (H. Geuze). Colocalization was evaluated on a Phillips transmission electron microscope by counting at least 100 gold-labeled membrane objects (as well as unlabeled objects) in each specimen.

Measurements of Tfn and dIgA Internalization, Recycling, and Transcytosis

MDCK cells were grown and seeded onto Transwell inserts as for density gradients except that 24-mm Transwell inserts were used with one-tenth the number of cells used for a 75-mm insert. Cells were induced and label bound to the basolateral surface at 0°C as for density gradients. After binding and washing, cells were warmed by addition of 37°C DMEM plus 100 μg/ml unlabeled Tfn to the upper chamber. After 1.5 min, this media was added to the lower chamber as well. The media from the upper and lower chambers was removed and replaced every 2 or 5 min for up to 90 min. Released ^{125}I-Tfn or dIgA was detected using a gamma counter (Beckman). In cases where the surface bound ligand was monitored, separate Transwell inserts were used for each time point. At the selected time, the Transwell was rapidly removed to ice-cold PBS^{2+} and acid washed as for density gradients. The acid and neutral washes were combined for counting. Transwell membranes were cut from the inserts and counted directly to determine the amount of internalized label either at a selected time point or at the end of a series of time points.

Modeling of Kinetic Data

Because Tfn and dIgA remain associated with their receptors throughout a single round of endocytosis, the presence of ligand could be used to follow the progress of receptors through the cycle. The association is essentially quantitative so that dissociation constants are not included in the model. Both Tfn and dIgA are released upon reaching the surface. In the case of Tfn, reuptake was prevented by using excess unlabeled Tfn.

Each data set was used individually for curve fitting and modeling. Kinetic values derived from each data set were then averaged to obtain the final rate constants. The models were based on the assumption that ligand moving from compartment A to compartment B does so in a first order manner with rate constant k (in units min^{-1}) so that:

$$A \xrightarrow{k} B$$

is represented as $dA/dt = kA$; conversely, $dB/dt = -kB$. Integrating this gives $ln(A_t/A_o) = -kt$, which converts to $A_t = A_o e^{-kt}$.

This final value represents the change in concentration of ligand in A over time t. Therefore, for ligand moving from A to B, the concentration of ligand in each after a unit of time is represented as $dA/dt = -kA$, integrated to give $A_t = A_o e^{-kt}$; $dB/dt = kA$, integrated to give $B_t = B_o + (A_o - A_o e^{-kt})$.

This equation can be carried on to multiple linked compartments $A^{-k1} \rightarrow B^{-k2} \rightarrow C$ where after time t, the concentration of ligand in each compartment can be represented in an already integrated form as: $A_t = A_o e^{-k1t}$; $B_t = B_o e^{-k2t} + (A_o - A_o e^{-k1t})$; and $C_t = C_o + (B_o - B_o e^{-k2t})$.

The implicit assumption in these equations is that material that departs A for B during a time interval will not be immediately available for reexport from B to C (or back to A for that matter) during the same time interval. This can be viewed physiologically as the time in which ligand is sorted into a transport vesicle but has not yet arrived at the destination compartment. This time interval was arbitrarily set to 0.16666 min which is rapid in comparison to recycling kinetics. The complete set of equations was then recalculated after each time increment. For the model of recycling and transcytosis, the variables were defined as: A, material bound to basolateral membrane; a, a specific subset of bound dIgA that does not internalize; B, first endosomal compartment; C, second endosomal compartment; D, basolaterally recycled ligand; E, apically released (transcytosed) ligand; k_1, rate of transport of ligand from A to B; k_{-1}, rate of transport of ligand from B to A; k_2, rate of transport of ligand from B to C; k_{-2}, rate of transport of ligand from C to B; k_3, rate of transport of ligand from C to D; k_4, rate of transport of ligand from B to D; k_5, rate of transport of ligand from C to E; k_6, rate of transport of ligand from B to E; k_7, rate of transport of ligand from a to D. The assignment of rate constants is graphically displayed in Fig. 6.

The equations describing transit of ligand were integrated as described above to yield the following algebraic forms for calculation:

$$A_t = A_o e^{-k1t} + B_o e^{-(k-1)t}$$

$$a_t = a_o e^{-k7t}$$

$$B_t = B_o(e^{-[(k-1)+k2+k4+k6]t}) + (A_o - A_o e^{-k1t}) + (C_o - C_o e^{-(k-2)t})$$

$$C_t = C_o(e^{-[(k-2)+k3+k5]t}) + (B_o - B_o e^{-k2t})$$

$$D_t = D_o + (B_o - B_o e^{-k4t}) + (C_o - C_o e^{-k3t}) + (a_o - a_o e^{-k7t})$$

$$E_t = E_o + (B_o - B_o e^{-k6t}) + (C_o - C_o e^{-k5t}).$$

These equations were entered into a spreadsheet program (Microsoft Excel 5.0) and used to model recycling and transcytosis. The initial values were set so that all of the internalized ligand started in compartment A (or a). In situations where some ligand was nonspecifically bound to the Transwell support (e.g., 5%) the starting value of compartment A could be set to 95%. Curves were manipulated by changing the values for the rate constants to fit each data set. The spreadsheet had a cumulative rounding error of <1.5%. To model a pathway that does not exist or is completely inhibited by a drug, the k for that pathway was set to zero. As may be expected, the early, middle, and late portions of curves representing transcytosis and recycling were differentially sensitive to changes in different rate constants, allowing derivation of unique solutions to each curve fitting situation.

Results

FITC Passes Sequentially through Peripheral-basolateral and Perinuclear-apical Endosomes in Polarized MDCK Cells

We and others have demonstrated the existence of distinct peripheral EE and perinuclear RE populations that label after the uptake of Tfn in nonpolarized CHO cells (Yamashiro et al., 1984; Daro et al., 1996). To confirm that analogous endosome populations exist in polarized epithe-

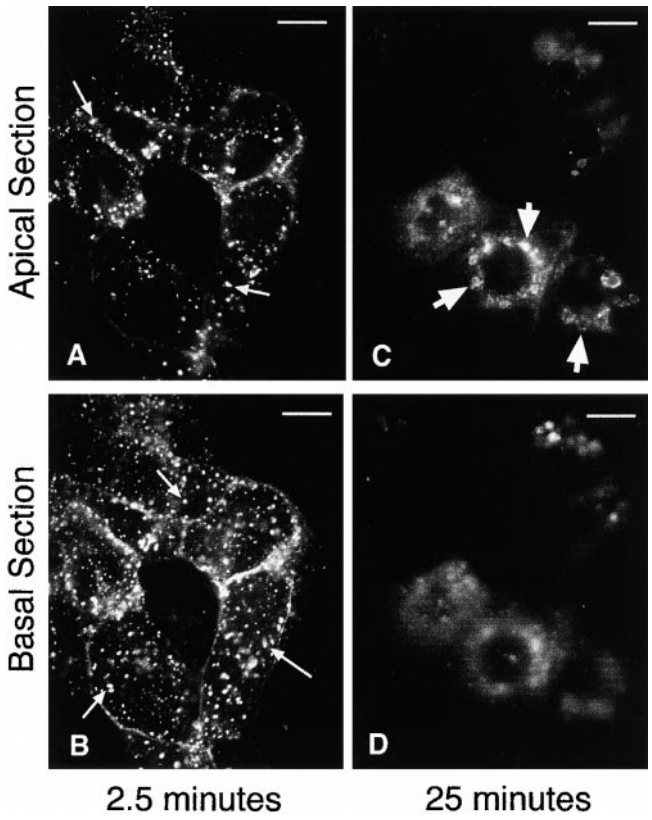

Figure 1. FITC-Tfn passes sequentially through peripheral and perinuclear endosomes in polarized MDCK cells. MDCK cells were transfected with the human TfnR and grown on clear Transwell filters. FITC-Tfn was bound to the basolateral surface at 0°C and internalized at 37°C for 2.5 min (A and B) or 25 min (C and D). Fluorescence images were obtained with focal planes at 4.5 μm (A and C) and 0.5 μm (B and D) from the filter surface. After 2.5 min, FITC-Tfn was localized in punctate basolateral structures in the basal and apical cytoplasm (A and B, arrows). By 25 min, the FITC-Tfn shifted to larger, more apical and perinuclear structures (C, arrows). Bar, 10 μm.

lial cells, we monitored the endocytosis of a synchronous pulse of FITC-Tfn by filter-grown MDCK cells transfected with the human TfnR. After FITC-Tfn was bound at 0°C, the cells were washed and then warmed to 37°C for 2.5–25 min to permit endocytosis. After fixation, deconvoluted optical sections were taken in the basal versus apical cytoplasm (0.5 vs. 4.2–4.5 μm from the filter surface, respectively). As shown in Fig. 1, after 2.5 min of uptake much of the FITC-Tfn was in small vesicles scattered throughout the basal cytoplasm (B) and, to a lesser extent, in the apical cytoplasm (A). After 25 min, less total FITC-Tfn remained and its distribution was markedly different. Most labeled structures were now found in the apical cytoplasm, clustered around the nucleus (Fig. 1 C, arrows). As compared with the pattern at 2.5 min, the basal cytoplasm was relatively devoid of labeling (Fig. 1 D). We operationally defined the vesicles labeled after 2.5 min as EEs and the apical structures labeled after the 25-min chase as REs. Identical results were obtained if the cells were pulsed and chased entirely at 37°C indicating that the differential localization of Tfn-containing endosomes was not induced by the temperature shift (not shown).

Resolution of EEs and Apical REs by Density Gradient Centrifugation

Although Tfn clearly labeled geographically distinct populations of vesicles at different times of uptake, this criterion alone cannot reliably distinguish between EE and RE populations. Even when supplemented by the immunofluorescence data showing a differential distribution of rab proteins between the two populations, the distinctiveness of compartments must be supplemented by physical separation. Thus, to determine if EEs and REs represent distinct compartments, we sought to separate them by cell fractionation.

^{125}I-Tfn was bound to the basolateral surface of filter-grown MDCK cells at 0°C and then internalized at 37°C in the presence of unlabeled Tfn for various times. At each time point, the cells were washed in low pH buffer (to remove surface bound ^{125}I-Tfn), homogenized, and postnuclear supernatants centrifuged for 20 h in preformed 5–20% Optiprep gradients. When cells were fractionated after 2.5 min of uptake, a major peak of ^{125}I-Tfn was observed at ~15% Optiprep (fractions 24–26). A minor lower density peak (fractions 6–9) was also observed. Since the low density peak comigrated with phosphodiesterase activity and with ^{125}I-Tfn from cell homogenized without warming, it was likely to represent remaining plasma membrane-bound ligand. Thus, the major peak (fractions 24–26) must represent the EE population.

When ^{125}I-Tfn was chased into the cells for 25 min before homogenization, centrifugation yielded a single peak that was shifted to a slightly lower density than the 2.5 min EE peak (Fig. 2). Since this second peak appeared at the expense of the EE peak and only after >20 min of chase, it was likely to correspond to the apical RE population in MDCK cells. Although the kinetically defined EE and RE peaks were not completely separated under the gradient conditions used, they were clearly resolved, demonstrating that EEs and REs are physically distinct entities.

EEs and REs Have Different Protein Compositions

We next characterized the EE and RE peaks using markers which might be differentially distributed between the two endosome populations. For this purpose, we centrifuged MDCK cell postnuclear supernatants on shallower 10–20% Optiprep gradients after labeling with ^{125}I-Tfn for 2.5 or 25 min. In addition, surface bound Tfn was not removed before homogenization in order to provide a convenient plasma membrane marker. Although both peaks were somewhat broader, EEs (2.5 min) were clearly detected at fraction 23 while REs (25 min) were at fractions 19–20 (Fig. 3 A).

The equilibrium distribution of the TfnR was probed by Western blot. As shown in Fig. 3 B (top row), most of the TfnR sedimented with REs (fractions 19–20) with a well resolved small peak in the low density region of the gradient (fractions 2–7). This low density peak was likely to reflect plasma membrane TfnR, as it cosedimented with membranes labeled when ^{125}I-Tfn was bound at the basolateral surface before homogenization. Thus, the majority

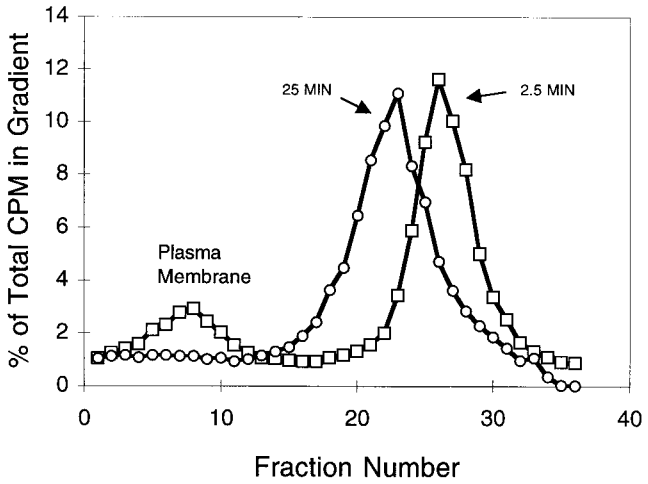

Figure 2. Separation of EEs and REs by Optiprep gradient centrifugation. MDCK cells transfected with the human TfnR were grown on Transwell filters. ^{125}I-Tfn was bound at 0°C and then internalized for either 2.5 or 25 min. The cells were acid washed to remove remaining surface bound ^{125}I-Tfn, homogenized, and postnuclear supernatants separated on 5–20% linear Optiprep gradients. The low density region of the gradients is on the left (fraction 1). ^{125}I-Tfn internalized for 2.5 min was contained within membranes which sedimented towards the bottom of the gradient (squares). After 25 min of chase, the Tfn was recovered as a single peak of slightly lower density (circles). The position of the plasma membrane was determined by alkaline phosphodiesterase activity and used to indicate the position of plasma membranes on the gradient. β-Hexosaminidase activity (lysosomes) formed a characteristically well defined peak in fractions 9–15 (not shown). The radioactivity in each fraction was normalized to percent total label loaded in each gradient (191,589 cpm for 2.5-min time point; 40,767 cpm for 25-min time point).

of the TfnR detected on the Optiprep gradients was associated with intracellular membranes, especially REs.

We next determined the distribution of rab4 and rab11, two rab proteins which have been associated with EEs and perinuclear REs by immunofluorescence. The presumptive EE marker rab4 was more closely associated with membranes labeled after the 2.5-min pulse of ^{125}I-Tfn, exhibiting a peak at approximately fraction 23 and clearly resolved from the major TfnR peak (Fig. 3 B, middle). rab11, on the other hand, did not cosediment with rab4-containing EEs and was instead shifted to lower density membranes overlapping with the major TfnR peak (fractions 19–20).

Although large fractions of rab4 and rab11 were detected in very low density regions (fractions 1–9), both rab proteins were judged to be soluble as they did not pellet after ultracentrifugation. In contrast, rab4 and rab11 in the endosome-containing fractions were quantitatively pelleted when centrifuged under identical conditions (not shown). We could not determine if the low density rab4 and rab11 reflected a large cytosolic pool in MDCK cells or if they were released upon homogenization (as are other peripheral proteins such as COPI and Arf). In either case, it is important to note that all of the membrane-associated rab4 and rab11 detected in the gradients cosedimented with the organelles with which they had been previously associated by immunocytochemistry.

To demonstrate that TfnR and rab4 (or rab11) were present in the same vesicles, membranes were recovered from Optiprep gradient fractions, immobilized on EM grids, and labeled with antibodies to rab4, rab11, or the cytoplasmic domain of TfnR (Fig. 3 C). Of the vesicles found that labeled with TfnR in fraction 24 of the EE peak, 63% were also positive for rab4 (TfnR labeled with 5-nm gold, small arrowheads; rab4 labeled with 10-nm gold, large arrowheads). 42% colabeled for TfnR and rab11 (10-nm gold, not shown). Approximately 40% of the vesicles in this fraction were positive for rab4 but negative for TfnR, presumably representing EEs depleted of TfnR. In the RE peak (fraction 27), 73% of the structures were double-positive for both TfnR and rab11, although 60% of the TfnR-positive vesicles were also positive for rab4. Only 16% of the structures in the RE peak labeled for rab4 alone, however.

Thus, the overlapping but distinct Tfn-containing EE and RE peaks comigrated differentially with rab4 and rab11, demonstrating that the two endosome populations are physically and biochemically distinct. As a result of the homogenization and fractionation procedures, nearly all of the vesicles recovered from the gradients exhibited a nondescript round morphology (as demonstrated in Fig. 3 C), preventing any further conclusions based upon either morphology or localization of the immunolabel within each vesicle. Consequently, it was of interest to determine if EEs and REs had distinct functional attributes.

AlF_4 Causes Transient Retention of FITC-Tfn in REs

To help clarify the relative functions of the two endosome populations, we sought to identify pharmacologic agents which selectively altered the transit of Tfn through either EEs or REs. Various potential inhibitors were screened for their ability to alter FITC-Tfn transport. We first used CHO cells since they organize their REs in a characteristic position directly over the nucleus (Daro et al., 1996). One useful agent was the phosphate transition state analogue AlF_4, a phosphatase inhibitor and agonist of various GTPases (Sternweis and Gilman, 1982), which appeared to slow the exit of Tfn from REs. This effect was illustrated in Fig. 4. When CHO cells (transfected with the human TfnR) were pulsed with FITC-Tfn for 30 min, various small peripheral and perinuclear structures were labeled (Fig. 4 A, panel A). These greatly decreased in intensity after a 30-min chase in unlabeled Tfn (Fig. 4 A, panel B). However, when the chase medium contained 30 μM AlF_4, the intensity of perinuclear labeling was significantly greater (Fig. 4 A, panel C).

Similar results were obtained for MDCK cells (Fig. 4 A, panels D–F), although AlF_4 treatment did not appear to cause as much intracellular "retention" of FITC-Tfn (see below), nor were the labeled endosomes as well organized in a perinuclear array as in CHO cells. However, as previously found for dIgA-containing REs, the FITC-Tfn–containing REs were concentrated in the apical cytoplasm as revealed by vertical (X-Z) confocal sections (Fig. 4 B). Moreover, fractionation on Optiprep gradients demonstrated that ^{125}I-Tfn remaining in MDCK cells chased in

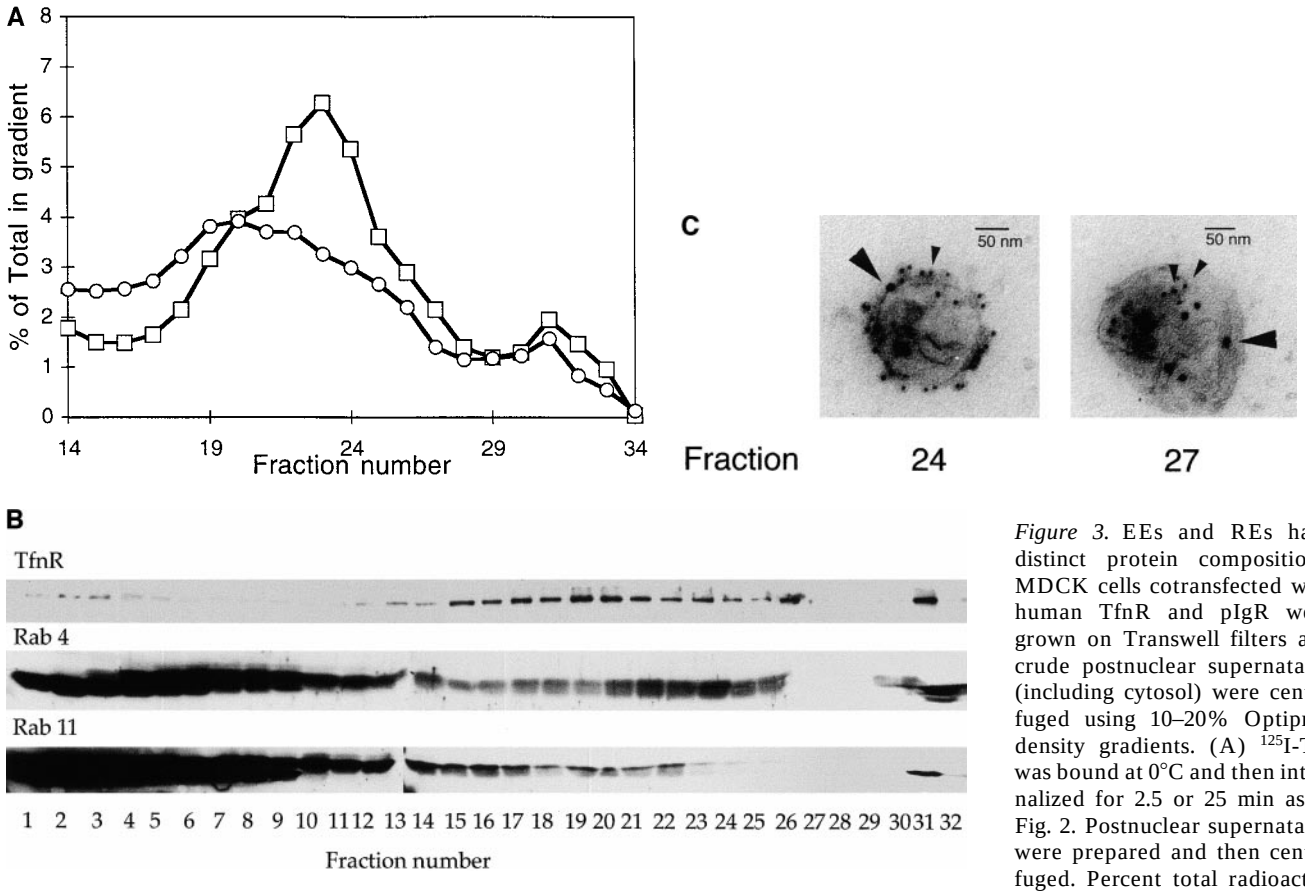

Figure 3. EEs and REs have distinct protein compositions. MDCK cells cotransfected with human TfnR and pIgR were grown on Transwell filters and crude postnuclear supernatants (including cytosol) were centrifuged using 10–20% Optiprep density gradients. (A) ^{125}I-Tfn was bound at 0°C and then internalized for 2.5 or 25 min as in Fig. 2. Postnuclear supernatants were prepared and then centrifuged. Percent total radioactivity in each gradient is indicated for the 2.5-min time point (squares) and the 25-min time point (triangles). ^{125}I-Tfn peaks around fraction 5 cosediment with the basolateral plasma membrane marker alkaline phosphatase; more ^{125}I-Tfn was found in this region than in Fig. 2 because cells were not extensively acid washed before homogenization. EEs are distinguished by a peak at fraction 23 and REs by a peak at fraction 20. (B) Western blots of fractionated cells using antibodies to human TfnR, human rab4, and human rab11. Half of the entire volume of each fraction was loaded in each lane. TfnR was found in all fractions but is most abundant in the RE-containing fractions identified by the 25-min ^{125}I-Tfn peak. rab4 cosedimented most closely with the EE peak; rab11 was relatively depleted from these EE-containing fractions relative to higher density fractions more coincident with REs (TfnR, 25 min ^{125}I-Tfn). (C) Double label immunoelectron microscopy of endosomes isolated on Optiprep density gradients. Tfn receptor was labeled with 5-nm gold in both images (small arrowheads). Fraction 24 was additionally labeled for rab11 with 10-nm gold (large arrowheads). Fraction 27 was labeled for rab4 with 10-nm gold (large arrowheads).

the presence of AlF_4 was limited to fractions characteristic of REs (Fig. 4 C). These fractions were also devoid of markers for the Golgi complex (e.g., mannosidase II, galactosyl transferase; not shown), indicating that AlF_4 did not cause Tfn transport into cisternal Golgi elements. Thus, in both CHO and MDCK cells, AlF_4 appears to cause a transient accumulation or retention of FITC-Tfn in REs.

AlF_4 Causes Missorting of Tfn Recycling in MDCK Cells

Quantitative measurements of Tfn recycling in AlF_4-treated cells confirmed the suggestion that the intracellular retention of Tfn was more pronounced in CHO than in MDCK cells. Whereas recycling was inhibited by ~30% after 2 h in CHO cells, in filter-grown MDCK cells the total amount of recycling into both the apical and basolateral media was inhibited by only ~10% (Fig. 5 A). However, there was a marked alteration in the polarity of recycling. Although ~95% of the internalized ^{125}I-Tfn was released back into the basolateral medium by control cells, when 30 μM AlF_4 was added during the recycling period, substantial amounts of ^{125}I-Tfn were now released into the apical medium (Fig. 5 B). This induction of basolateral to apical transcytosis involved up to 20% of the total internal ^{125}I-Tfn after 40 min of chase, as compared with <5% transcytosis in control cells. Since AlF_4 may act preferentially at the level of REs, REs may thus be an important site for polarized sorting.

Kinetic Analysis Suggests That All Tfn Does Not Proceed from EE to RE before Reaching the Basolateral or Apical Surfaces

To address the relative contributions of EEs and REs in polarized receptor recycling, we performed detailed kinetic analysis of basolateral recycling and transcytosis us-

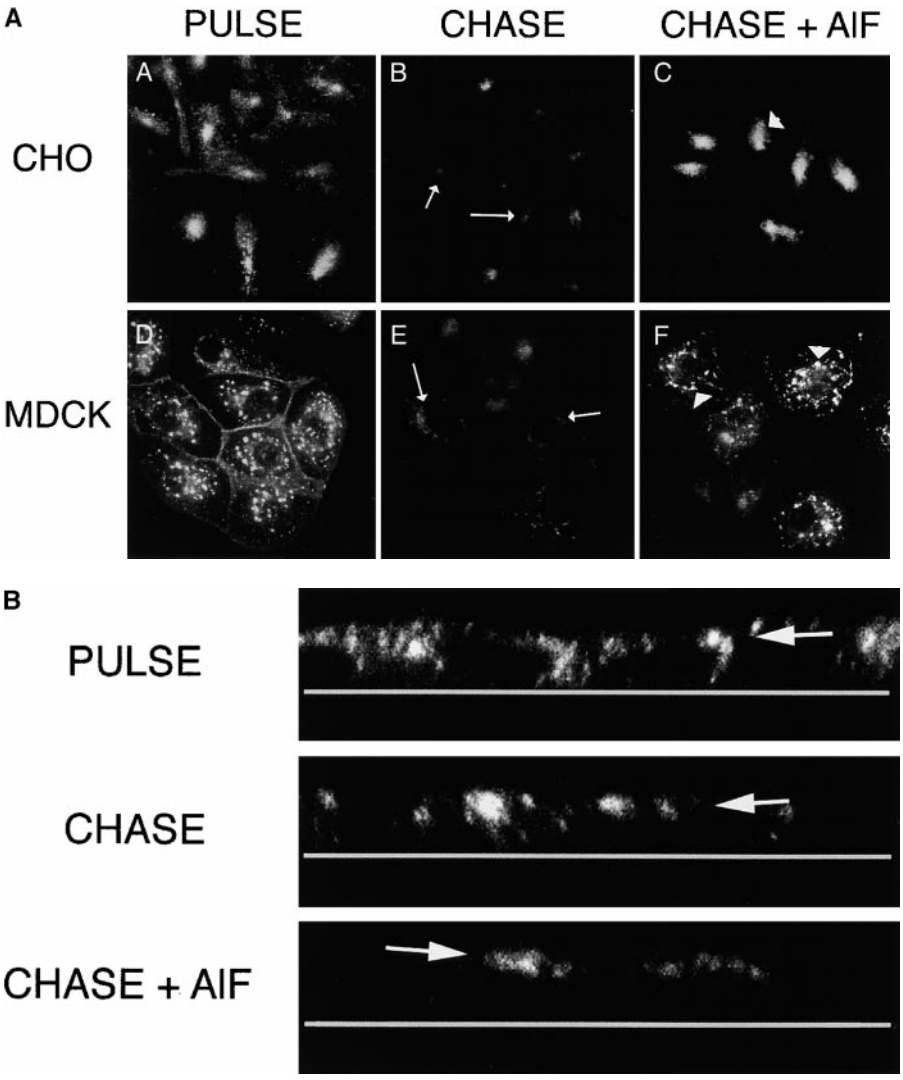

Figure 4. Partial retention of FITC-Tfn in REs by AlF_4. (A) CHO cells and MDCK cells expressing human TfnR were pulsed with FITC-Tfn for 30 min at 37°C, conditions which labeled both peripheral and perinuclear endosome populations (panels A and B). The cells were then chased in the presence of excess unlabeled Tfn for 30 min (panels C and D). Although a few cells remained brightly labeled, most exhibited a marked loss of FITC-Tfn, with remaining cell-associated FITC-Tfn found predominantly in perinuclear vesicles (arrows). When cells were chased in the presence of unlabeled Tfn and AlF_4 for 30 min, however, FITC-Tfn was largely retained in the perinuclear endosomes (panels E and F). In CHO cells, these structures exhibited the characteristic distribution as a tightly organized array near the microtubule organizing center; in MDCK cells, they were more diffusely distributed, but nevertheless closely apposed to the nucleus. (B) X-Z reconstructions from confocal fluorescence imaging of intact, fully polarized monolayers of MDCK cells transfected with the human TfnR. Cells were loaded with FITC-Tfn for 20 min at 37°C (top). The cells were chased in the presence of unlabeled Tfn for 40 min in the absence (middle) or presence (bottom) of AlF_4. Arrows indicate the apically located FITC-Tfn–containing endosomes; gray lines indicate the position of the Transwell filters and thus the basolateral surface of the cell monolayer. Each panel has been contrast processed with Adobe Photoshop to emphasize the position of the label rather than the total amount. (C) Optiprep gradient centrifugation of MDCK cells after ^{125}I-Tfn uptake for 2.5 min (squares) or 25 min (circles) in the presence (closed symbols) or absence (open symbols) of AlF_4. Low density fractions are shown to the left.

ing MDCK cells stably transfected with both human TfnR and rabbit pIgR (Mostov et al., 1984; Schaerer et al., 1990). ^{125}I-Tfn was bound to the basolateral surface at 0°C, and after rinsing the filter-grown monolayers were shifted to 37°C in the presence of excess unlabeled Tfn to prevent reinternalization. At 1–5-min intervals, the appearance of ^{125}I-Tfn in the apical medium (transcytosed) or basolateral medium (recycled) was followed, as was the presence of acid-sensitive ^{125}I-Tfn still bound to receptors on the basolateral surface (Podbilewicz and Mellman, 1990). For some experiments, 30 μM AlF_4 was included during the 37°C incubation. The data were analyzed using a series of

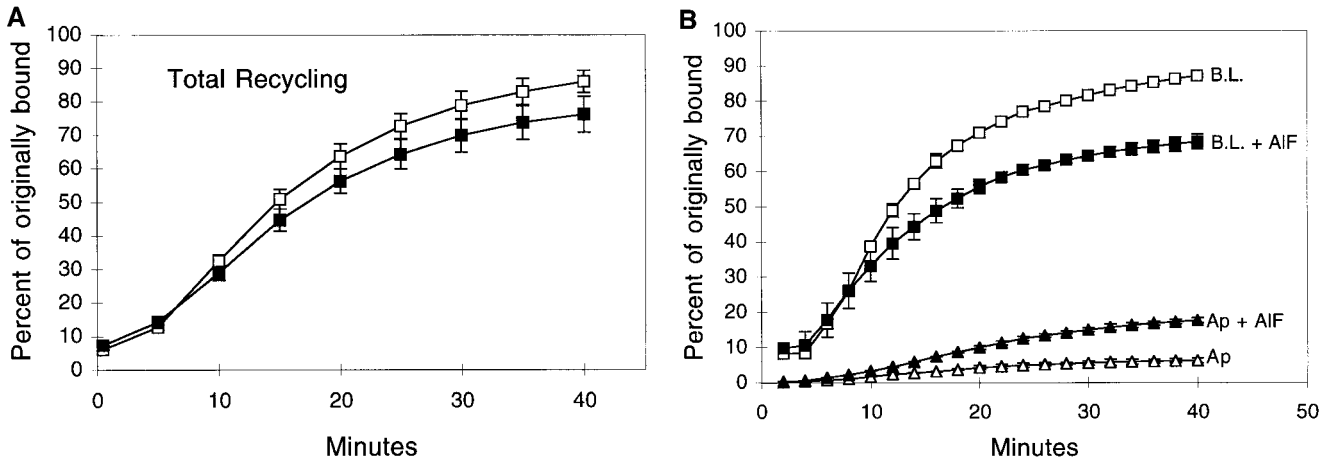

Figure 5. AlF_4 causes missorting during Tfn recycling in MDCK cells. (A) MDCK cells transfected with the human TfnR were grown on Transwell filters. ^{125}I-Tfn was bound to the basolateral membrane on ice. Cells were warmed to 37°C to initiate endocytosis. Appearance of total label in both the apical and basal media was combined and shown in the presence (closed squares) or absence (open squares) of AlF_4 ($n = 3$ for each condition). (B) Experiment as in A except that media was collected separately from the upper chamber (transcytosis, triangles, $n = 2$) or lower chamber (recycling, squares, $n = 4$ for AlF_4, $n = 3$ for control) in the absence (open symbols) or presence (closed symbols) of AlF_4. Error bars represent standard deviation when $n > 2$ or standard error when $n = 2$.

conventional mathematical models describing the transport of Tfn as a series of first order rate constants connecting the apical and basolateral surfaces with various internal compartments (equations in Materials and Methods) (Besterman et al., 1981; Wiley and Cunningham, 1982; Ciechanover et al., 1983; French and Lauffenburger, 1997).

We first determined the rate of internalization of surface bound ^{125}I-Tfn by measuring the disappearance of ^{125}I-Tfn that was sensitive to removal by acid stripping, as well as the appearance of ^{125}I-Tfn in the media and acid-insensitive ^{125}I-Tfn associated with the cells. Based on computer analysis of the kinetic data obtained (see Materials and Methods), we derived a rate constant for internalization of 0.21 $min^{-1} \pm 0.0077$, similar to other cell types (Ciechanover et al., 1983). There was no dissociation of Tfn into the medium, nor was the internalization rate altered by AlF_4 (not shown).

We also measured the polarized recycling of ^{125}I-Tfn by monitoring its appearance in the apical or basolateral media at 2-min intervals. These data were compared with a simple kinetic model in which the intracellular transit of Tfn followed the "single" pathway generally thought to be followed by recycling receptors: internalization and delivery to EEs, from EEs to REs, and from REs back to the plasma membrane (basolateral or apical). Reversible rate constants were assigned to each of these steps (Fig. 6 A). In the case of the initial internalization step (k_1), the reverse rate (k_{-1}) would account for the possibility that some internalized Tfn–TfnR complexes might be recycled without reaching an acidified compartment and thus would remain receptor-bound after returning to the surface. Transit of Tfn to LEs and lysosomes was assumed not to occur, as shown previously (Schmid et al., 1988).

By systematically varying the values for each forward and reverse rate constant (holding k_1 at its experimentally determined value), predicted curves for basolateral and apical recycling were obtained and compared with the actual data (Fig. 6 B; data as individual points). Curves generated by these equations were fit to experimental data sets so as to minimize the sum of the squared differences (SS) between predicted and experimental values (Motulsky and Ransnas, 1987).

For control cells (Fig. 6 B, open symbols), the best fit curves matched the recycling and transcytosis data reasonably well, although there were slight variations between data and prediction (SS = 336 where SS = 0 is a perfect fit). More striking were the deviations between predicted curves and actual data in cells treated with AlF_4 (closed symbols). In this case, the best curve yielded SS = 836. Regardless of the combination of values employed for each of the rate constants, predicted curves for basolateral recycling never corresponded to the actual kinetics of recycling. Placing additional endosome compartments in series along a single pathway together with EEs and REs only served to further degrade the degree of curve fitting for both control and AlF_4-treated cells (not shown).

Thus, particularly in AlF_4-treated cells, the widely assumed pathway of sequential transport of Tfn from plasma membrane to EEs, to REs, and then back to the plasma membrane did not fit a kinetic representation of the data. Similar results were obtained for endocytosis and recycling in nonpolarized CHO cells (not shown).

EEs and REs Serve as Tandem Sorting Stations during Tfn Recycling

Since a single pathway involving obligatory transit from EEs to REs before recycling did not yield kinetics that optimally matched the data, we asked whether recycling might occur directly from EEs as well. To test this possibility, we introduced a single additional rate constant, k_4, to describe a potential rapid recycling pathway from EE directly back to the plasma membrane (Fig. 6 C). Again, by

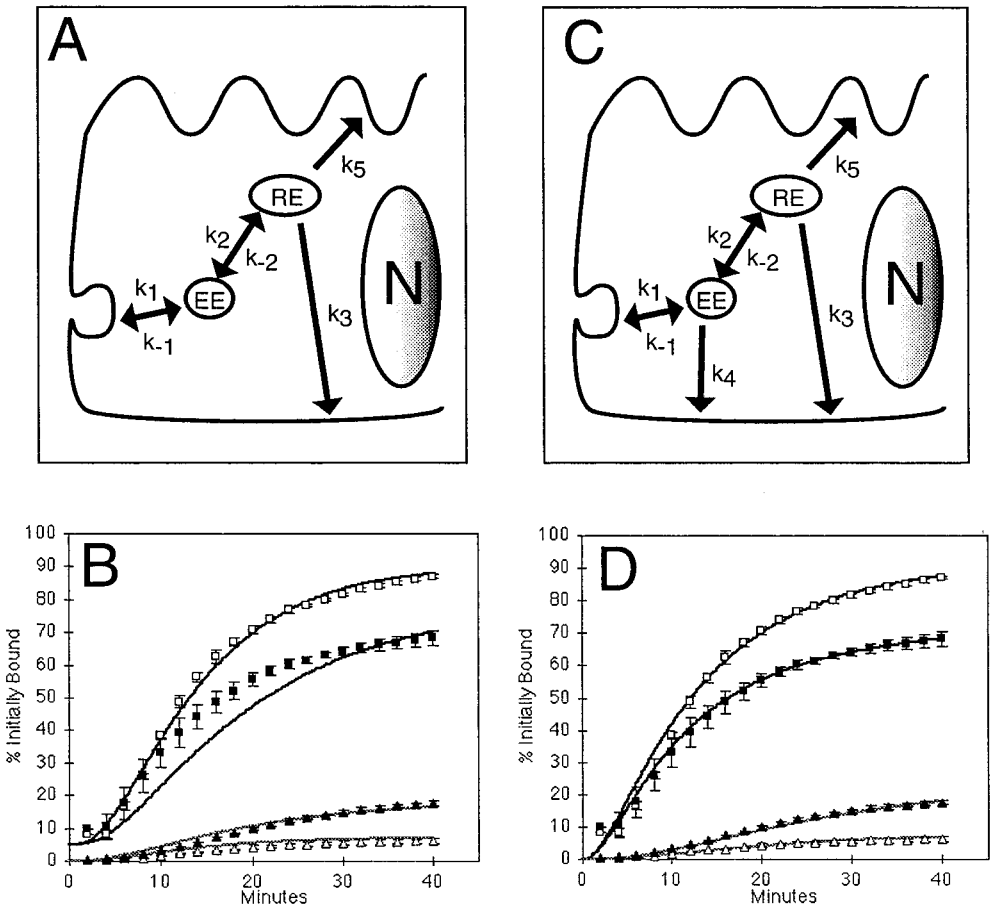

Figure 6. The kinetics of Tfn recycling in MDCK cells is consistent with the existence of two distinct endosomal recycling compartments. (A) A kinetic model of endocytosis assuming a single pathway through two consecutive internal compartments. First order rate constants (k_n) for passage of ligand along a given pathway segment are shown. k_n represents anterograde transport, while k_{-n} represents retrograde transport. (B) Best fit of the single pathway model was optimized by minimizing the value of the sum squared variances between predicted and experimental values. Data points (open square, control recycled; open triangle, control transcytosed; closed square, AlF_4 recycled; closed triangle, AlF_4 transcytosed) represent the actual experimental data to which curve fitting was attempted. Solid lines were derived from the mathematical model (black lines are recycled ligand, gray transcytosed ligand, solid lines are control cells, dashed are AlF_4 treated). Note the relatively poor fit of the model to recycled Tfn in AlF_4-treated cells (SS = 334 untreated, SS = 836 treated). (C) Addition of rate constants describing potential pathways from EEs direct to the basolateral plasma membrane (k_4) or the apical plasma membrane (k_6). (D) Fitting of the modified model described in C to experimentally determined data points. As in B, symbols represent the data and lines are generated from the modified model. The degree of fit was far better (Fischer's F-test of comparative fit: F = 48 for control, 424 for AlF_4; $P < 0.05$ for both, see text) than in B (SS = 140 untreated, SS = 64 AlF_4-treated).

systematically varying each rate constant, it was possible to identify solution sets which more accurately reflected the recycling and transcytosis data in control cells (SS = 140) and even cells treated with AlF_4 (SS = 64) (Fig. 6 D). The fit of the two-pathway model versus the one-pathway model was tested using Fischer's F-test for goodness of fit where $F = ([SS_1 - SS_2]/[df_1 - df_2])/(SS_2/df_2)$ (Daniel, 1987; Motulsky and Ransnas, 1987). SS refers to the sum of the squares of the variance at each data point and df refers to the degrees of freedom (number of data points minus number of nonfixed pathway values). For the two-pathway model as compared with the one-pathway model in control data F = 48 and for the comparative fits of AlF_4-treated cell data F = 424. For the 40 data points in each set, 5 independent kinetic parameters in the single model and 6 independent kinetic parameters in the two-pathway model $P < 0.005$ when F > 11.46 (Daniel, 1987). Thus, the addition of the second pathway gave a significantly better fit to the data than did the single pathway model.

Table I summarizes the predicted rate constants used to generate the optimized curves. The most remarkable feature was the finding that the unique best solution for the Tfn recycling and transcytosis data in AlF_4-treated cells required setting the rate of RE to basolateral transport (k_3) to zero. Any non-zero value for k_3 predicted much greater slopes for Tfn recycling after 30 min than were actually observed. Non-zero values for k_3 also produced curves con-

Table I. Mathematically Derived Rate Constants for Tfn and dIgA Recycling and Transcytosis

Rate constant (min^{-1})	Tfn control	Tfn AlF_4	IgA
k_1	0.21 ± 0.0077	0.21 ± 0.0083	0.22 ± 0.015
k_{-1}	0.028 ± 0.0039	0.026 ± 0.0041	0
k_2	0.087 ± 0.011	0.077 ± 0.0051	0.19 ± 0.0034
k_{-2}	0.023 ± 0.0099	0.026 ± 0.0099	0.095 ± 0.060
k_3	0.057 ± 0.014	0	0
k_4	0.11 ± 0.020	0.097 ± 0.020	0.095 ± 0.027
k_5	0.018 ± 0.0056	0.027 ± 0.0028	0.022
k_6	0	0	0.012 ± 0.011
k_7	0	0	0.75

The rate constants are all first-order rates determined for passage between endocytic compartments as illustrated in Fig. 6 C. For each constant, the mathematical model was fit to multiple data sets to derive rate constants for each data set. The value given is the mean value derived from all data sets with the error defined as the standard deviation of those values. Note the reduction of k_3 to zero in both AlF_4-treated cells recycling Tfn, and in IgA transport. All dIgA data were obtained in the absence of AlF_4.

taining lower levels of Tfn retained intracellularly or recycled apically than were obtained experimentally.

With k_3 at zero, a rate constant for direct recycling from EE (k_4) was calculated to be 0.097 min^{-1} ± 0.020 (Table I). Thus, a considerable fraction of the basolateral recycling that occurs in AlF_4-treated cells was predicted to come directly from EEs. The remaining rate constants were derived by placing further constraints on the construct, forcing it to account at each time point for the rate and extent of apical recycling (transcytosis), and the amounts of Tfn remaining intracellularly, basolaterally recycled, and remaining on the basolateral surface. Using these constraints, we derived a unique solution for the rate of Tfn transport between EEs and REs (k_2 = 0.077 min^{-1} ± 0.0051 and k_{-2} = 0.026 min^{-1} ± 0.010). Interestingly, these values are similar to those derived from video microscopic measurements of transfer between geographically defined REs and EEs in CHO cells (Ghosh and Maxfield, 1995).

We considered a possible contribution of a pathway (k_6) from EEs directly to the apical surface, particularly in AlF_4-treated cells. However, setting non-zero values for k_6 produced curves that fit less well than the unique solution provided by setting k_6 to 0 and k_5 to 0.027 min^{-1} ± 0.0028.

In untreated control cells, the best curve fits were obtained using non-zero values for k_3. Systematic generation of progress curves produced a value of 0.057/min ± 0.014 for k_3. Remarkably, this was the only major difference between control and treated cells. The derived value in control cells for k_4, direct recycling of Tfn from EE to the basolateral medium, was 0.11 min^{-1} ± 0.020, only slightly higher than that derived in the presence of AlF_4 (k_4 = 0.097 min^{-1}) (Table I). This suggested that AlF_4 partially inhibited recycling from EEs, but nearly as much as from REs. It was also of interest that the calculated rate constant for transport from REs to the apical plasma membrane (k_5) in control cells was comparable to that obtained in AlF_4-treated cells, despite the fact that AlF_4 greatly increased the apical transcytosis of Tfn. Thus, the ability of AlF_4 to enhance transcytosis appears to result more from the selective inhibition of Tfn transport from REs to the basolateral surface than from an enhancement of endosome to apical membrane transport.

Testing the Model's Predictions

The kinetic model of Tfn recycling was derived from measurements of ^{125}I-Tfn that was released apically, released basolaterally, remained bound to the basolateral surface, or was otherwise cell associated. Due to inaccuracies inherent in determining amounts of ^{125}I-Tfn in overlapping gradient fractions, we did not attempt to determine quantitatively the amounts of Tfn in EE and RE by cell fractionation at each time point. However, the model simulates passage through EEs and REs and thus makes specific qualitative predictions about the Tfn passage through these compartments. As shown in Fig. 7 A, EEs were predicted by the model to fill maximally at 5 min, as compared with 12–13 min for REs. At 2.5 min, the model predicted that >90% of the Tfn remaining in the cell will be in the EEs. At 25 min, although much of the Tfn would have already left the cell, the model predicted that >66% of the remaining intracellular Tfn was in REs. These predictions were in accord with the fluorescence microscopy (Fig. 1) as well as the cell fractionation (Fig. 2) data.

AlF_4 treatment provided an additional way to check these predictions empirically. According to the model, there should be little change in the levels of Tfn in EEs, but at 30 min there would be a doubling of the Tfn remaining in the REs (Fig. 7 B). This prediction is borne out by the observation (in Fig. 3) that AlF_4 treatment caused selective if transient retention of FITC-Tfn in the REs. Additionally, the mathematical model predicts that AlF_4 will not alter the passage through the EE nor the nature of the compartments, a prediction confirmed by the subcellular fractionation of AlF_4-treated cells (Fig. 4 C).

Thus, specific predictions of the model concerning the intracellular localization of Tfn at different time points could be confirmed by the fluorescence microscopy and cell fractionation data, neither of which was used in formulating the model.

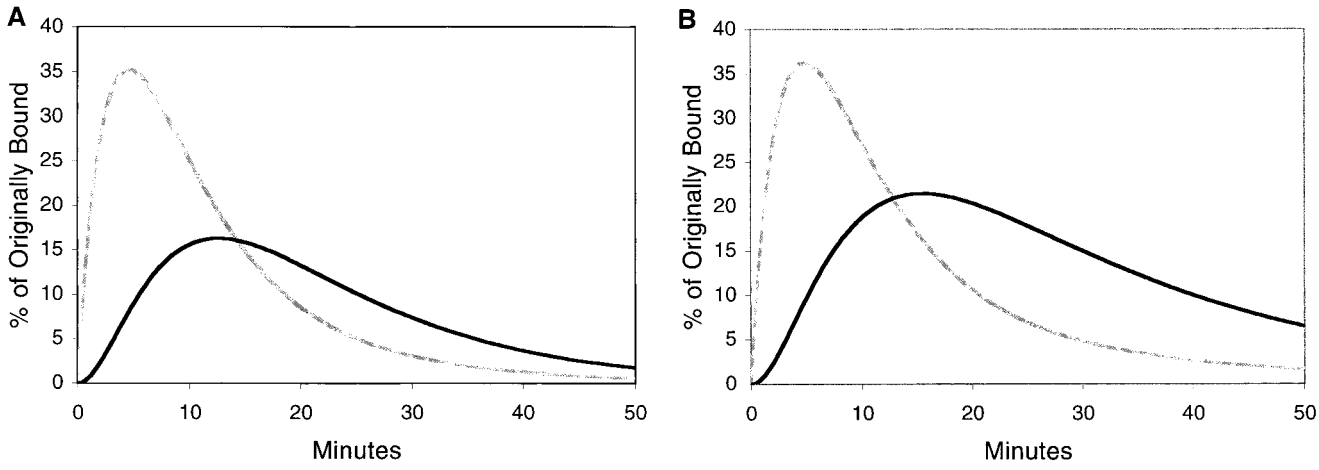

Figure 7. Predicted kinetics of appearance of Tfn in EEs and REs. (A) Using the mathematical model described in Fig. 6, C and D, the predicted amounts of Tfn in the EEs (gray line) and REs (black line) are shown over the course of the experiment in untreated cells. (B) Predicted Tfn amounts of Tfn in EEs and REs as in A but now in the presence of AlF_4. EE (gray line) and RE (black line) are shown. Note the increased duration of Tfn in REs as compared with controls (A).

Transcytosis of dIgA by MDCK Cells Involves Two Distinct Endosomal Compartments

A limitation of the analysis using Tfn recycling was that much of our ability to kinetically dissect two recycling pathways was based on alterations due to AlF_4 treatment. We next examined the model's ability to describe the behavior of pIgR-bound dIgA, a ligand which is normally (i.e., in the absence of AlF_4) subject to recycling as well as transcytosis (Casanova et al., 1990; Hunziker et al., 1991). Since the MDCK cells used for the Tfn uptake experiments were doubly transfected with pIgR, we were able to use the same cells for both ligands.

In MDCK cells transfected with only the pIgR, basolaterally applied dIgA passed through endosomes accessible to Tfn internalized to equilibrium (Apodaca et al., 1994). We first established that the pIgR in the double transfectants behaved as did MDCK cells expressing only the pIgR. To monitor transcytosis, polarized filter-grown monolayers were allowed to internalize ^{125}I-labeled human dIgA from the basolateral side for 10 min at 37°C, washed, and then recultured in the absence of ^{125}I-dIgA for an additional 60 min. In agreement with previous results, ~50% of the internalized ^{125}I-dIgA appeared by transcytosis in the apical medium by this time point (not shown) (Breitfeld et al., 1990; Hunziker et al., 1991).

Next, FITC-Tfn and Texas red–dIgA (TR-dIgA) were bound to the basolateral surface on ice, and the two ligands then were internalized for 2.5 or 25 min. In cells expressing both receptors, at 2.5 min FITC-Tfn and TR-dIgA colocalized in basolateral EEs (Fig. 8 A, top row, ar-

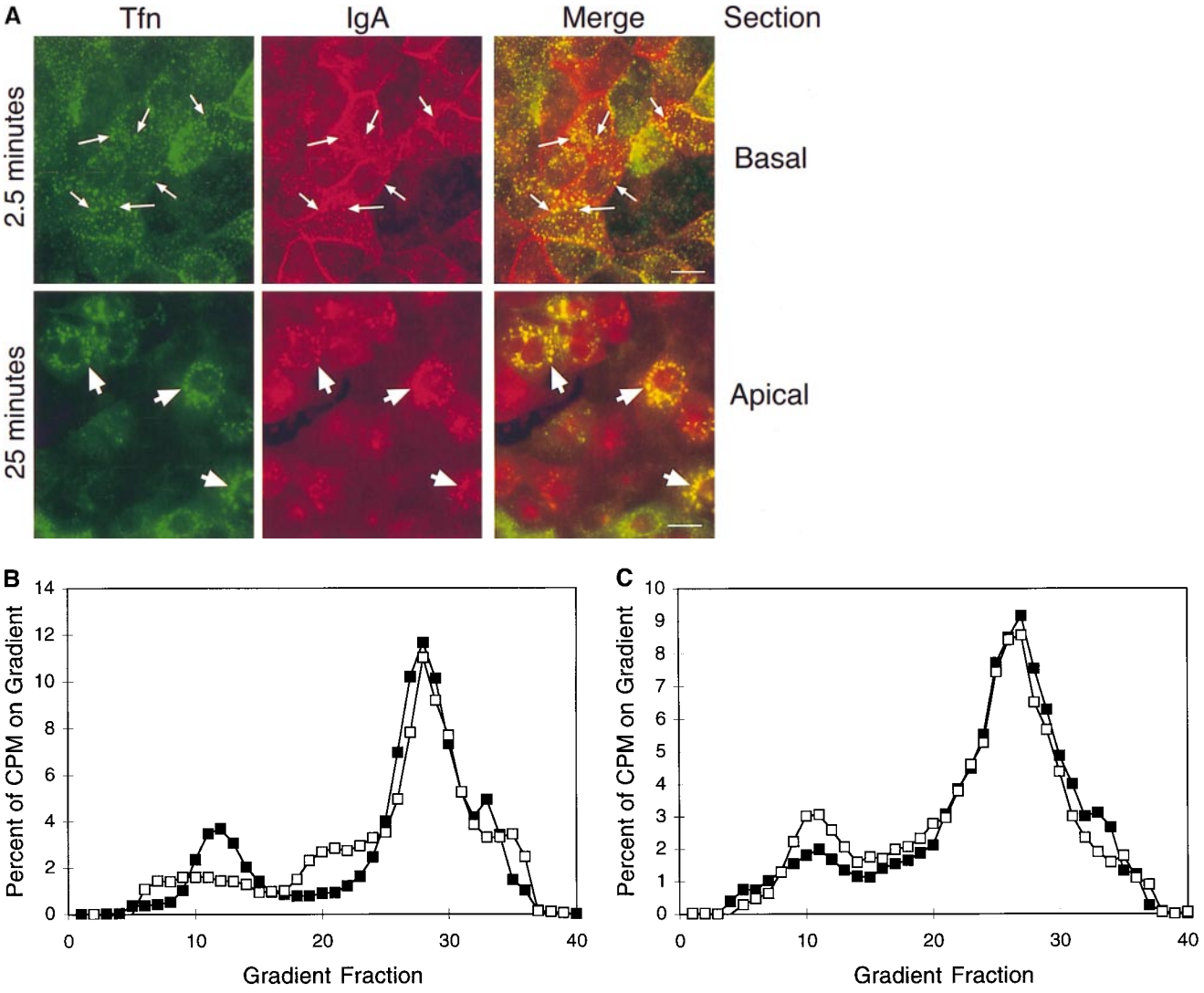

Figure 8. Tfn and dIgA transit through the same EE and RE populations. (A) FITC-Tfn and Texas red–dIgA were bound to the basolateral surface of MDCK cells doubly transfected with the TfnR and pIgR at 0°C. The ligands were then internalized at 37°C for 2.5 (top) or 25 min (bottom). Tfn (green) and dIgA (red) were imaged separately and merged; yellow spots indicate likely double-positive structures. 2.5-min images were taken 0.5 μm from the filter surface; 25-min images were taken ~5 μm from the filter surface, in the apical cytoplasm. Bar, 10 μm. (B) ^{125}I-Tfn or ^{125}I-dIgA were bound to the basolateral surface of filter-grown MDCK cells doubly transfected with TfnR and pIgR at 0°C. The ligands were internalized at 37°C for 2.5 min, then the cells were harvested and homogenates were fractionated in parallel on Optiprep density gradients. EE peak is at fraction 29. (C) After 25 min of internalization, both Tfn and dIgA shifted to apparently the same, less dense RE compartment. Closed symbols indicate Tfn, open symbols indicate dIgA.

rows). After 25 min, both ligands were colocalized in more perinuclear, apical REs (Fig. 8 A, bottom row, arrows).

Cell fractionation was used to confirm the fluorescence microscopy. ^{125}I-dIgA and ^{125}I-Tfn were bound to the basolateral surface of MDCK cells as above. After 2.5 or 25 min of uptake, cell homogenates were prepared and centrifuged on Optiprep gradients. ^{125}I-dIgA was transferred between vesicle populations that cosedimented with Tfn-containing EE and RE both after 2.5 min (Fig. 8 B) and 25 min (Fig. 8 C) of chase, again suggesting that Tfn and dIgA transit through the same endosomal populations.

Kinetic Analysis of dIgA Recycling and Transcytosis Reveals Specific Differences from the Tfn Pathway

We next measured transcytosis of ^{125}I-dIgA prebound at 0°C. Under these conditions, only 25% of the initially bound ^{125}I-dIgA appeared in the apical medium since at least half of the bound ^{125}I-dIgA dissociates into the basolateral medium before endocytosis. Since this process would affect the kinetic analysis of recycling, we first examined the rates of ^{125}I-dIgA internalization and dissociation (Fig. 9 A). The rate of internalization was determined by measuring the amount of ^{125}I-dIgA becoming resistant to acid stripping at 1-min intervals after warm up. The rate of dissociation was determined by measuring release of ^{125}I-dIgA into the basolateral medium. 45% ± 3.7% of the bound ^{125}I-dIgA was in the internalizable pool, while 51% ± 2.7% was in the pool of IgA which dissociated before internalization. It was possible that internalized and dissociated dIgA originated from a single pool of surface bound dIgA. However, the comparative fit of the two-pool model to a one-pool model using the dIgA internalization data with Fischer's F-test as above yields F = 1200 (for F > 3.89, the value of $P < 0.005$) clearly providing a significantly better fit for the two-pool model of dIgA binding. From these data, we could calculate an internalization rate constant (k_1) of 0.202 ± 0.011 min^{-1}, and more rapid rate of ^{125}I-dIgA dissociation into the basolateral medium (k_7) of 0.712 ± 0.13 min^{-1}. The rate of ^{125}I-dIgA internalization was indistinguishable from that for Tfn (Table I).

Having determined the rate at which IgA dissociated without internalization, it was now possible to dissect this effect from recycling of internalized IgA into the basolateral medium. After binding of ^{125}I-dIgA as above, the cultures were warmed and the amount of ^{125}I-dIgA in the medium determined every 30 s (Fig. 9 B). Over the course of 8 min, a biphasic curve was apparent. During the first 2.5 min, ^{125}I-dIgA appeared in the basolateral medium at the same rate calculated for rapid dissociation from the receptor (designated as k_7 = 0.712 min^{-1}). However, by 4 min, the rapid rate of ^{125}I-dIgA appearance had ceased but radioactivity continued to accumulate in the basolateral medium. Analysis of this slow phase of ^{125}I-dIgA release over the next 4 min yielded a single rate constant of 0.095 ± 0.027 min^{-1}. Assuming that recycling at times <8 min resulted from recycling out of EEs rather than the REs, we presume that this rate must describe k_4, the rate of dIgA recycling from EEs. Interestingly, this experimentally obtained value was very similar to the calculated value for Tfn recycling (Table I).

Using the measured values for internalization, dissocia-

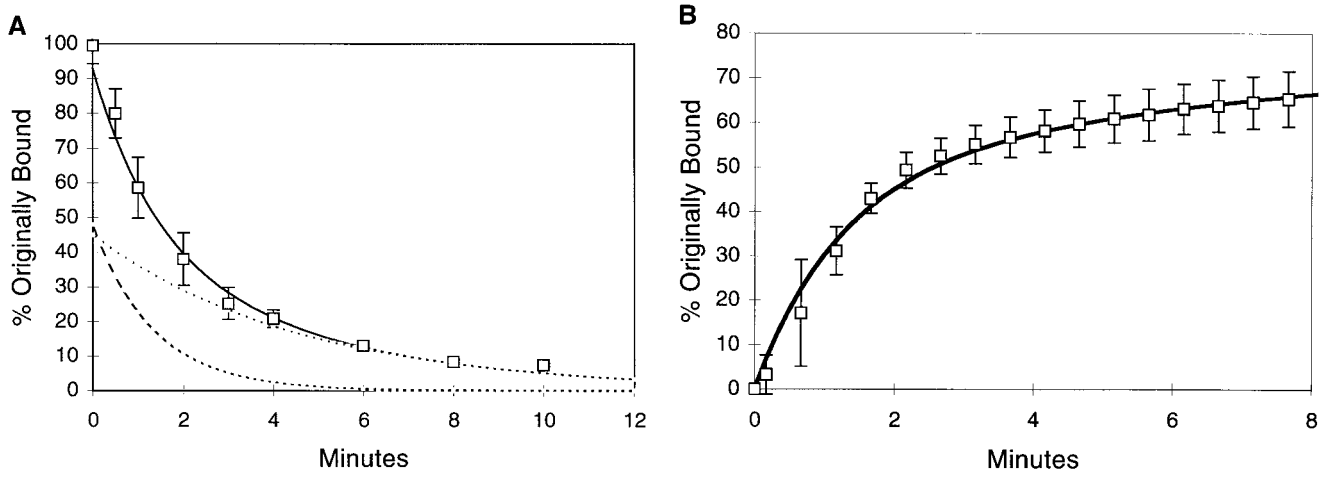

Figure 9. Kinetic analysis of dimeric IgA internalization. (A) Dissecting the contribution of rapid dIgA dissociation from internalization. MDCK cells transfected with the rabbit pIgR cDNA were grown on Transwell filters. ^{125}I-dIgA was bound to the basolateral surface on ice. The cells were warmed to 37°C, and at 2-min intervals individual filters were removed to ice-cold buffer and surface IgA stripped with a pH 2.9 wash. Disappearance of the acid sensitive counts (squares, $n = 3$) is a direct measure of dIgA clearance from the basolateral surface. Mathematically derived curves for dissociation (dashed line) and internalization (dotted line) were added together to get the mathematically predicted rate of surface clearance (solid line) which is compared with the experimentally derived values (in this model internalization and dissociation are from distinct pools of dIgA, SS = 104, see text). All counts were normalized to a percentage of counts initially bound to each Transwell filter. Error bars represent standard deviation. (B) The kinetics of dIgA recycling into the basolateral medium for early time points was plotted after correcting for the rapid dissociation of dIgA from pIgR before internalization (A). Open squares represent individual data points indicating the percentage of radioactivity initially bound. Line represents results of a mathematical model including both direct fall-off from the basolateral membrane into the basolateral media and recycling of internalized ligand from the EE to the basolateral media. The same kinetic rate constants used in A are used in B (SS = 63).

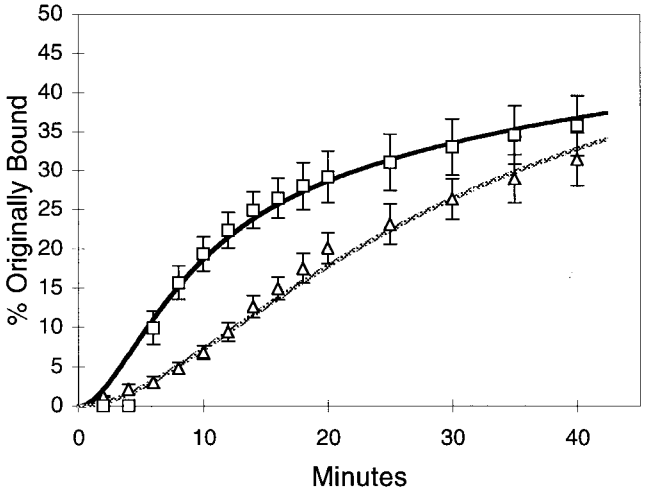

Figure 10. The two-compartment, two-pathway model developed for Tfn accounts for observed kinetics of IgA recycling and transcytosis. Corrected experimental data points for basolateral recycling (squares) and apical transcytosis (triangles) are shown and compared with best fit curves calculated using the model described in Fig. 6 C. Curves resulting from modeling of the data fit closely, suggesting that this model is consistent with the data (SS = 20, F = 83 compared with a single pathway).

tion, basolateral recycling, and transcytosis, we subjected the dIgA data to the same kinetic analysis as performed for Tfn. Again, the data were best described by the two-compartment pathway (Fig. 6 C). In other words, the model in which basolateral recycling or apical transcytosis can occur from either EEs or REs provided kinetic curves which fit the data extremely well (SS = 19.6) (Fig. 10), far better than curves obtained assuming that recycling and transcytosis can only occur after transfer to REs from EEs (F = 82.9; for seven parameters in this dual pathway model and six in the single pathway model, when $F > 9.1$, the value of $P < 0.005$). The most significant result was that the derived rate constant for recycling from RE to the basolateral medium (k_3) was zero, as calculated for Tfn recycling and transcytosis in AlF_4-treated cells (Table I). The model would predict that AlF_4 would have no effect on dIgA recycling or transcytosis; this was indeed the case when tested experimentally (not shown).

A comparison of the rate constants obtained for dIgA in untreated cells and for Tfn in AlF_4-treated cells yielded few other significant differences (Table I). The predicted rate of anterograde and retrograde transport between EEs and REs was increased, possibly suggesting that dIgA and Tfn may be sorted differentially in both compartments. Moreover, the model predicted a low level of EE to apical plasma membrane transport (k_6) which was not seen for Tfn with or without AlF_4.

Thus, a two-compartment model can be used to accurately describe the endocytosis, recycling, and transcytosis of dIgA. The data also suggest that the ability of AlF_4 to increase Tfn transcytosis may in effect phenocopy a physiological significant sorting mechanism which enhances dIgA transcytosis by blocking dIgA entry into the same basolateral pathway inhibited by AlF_4.

Discussion

It has long been appreciated that receptor recycling in polarized and nonpolarized cells alike involves two spatially distinct populations of endosomes, referred to here as EEs and REs (Mellman, 1996). However, why this should be the case has never been clear, nor have the relative roles of EEs and REs in the recycling pathway been firmly established. Recent immunofluorescence evidence has suggested that the two populations differ in their rab protein compositions. In addition, given that REs rarely contain fluid phase markers of endocytosis, there is good reason to believe that they represent structures that occur after EEs have sorted receptors destined for recycling from dissociated ligands destined for transport to LEs and lysosomes. Beyond these features, however, the relationship between EEs and REs has remained elusive.

In this paper, we have presented three lines of evidence that REs and EEs represent distinct populations, which can be resolved physically (by centrifugation), biochemically (by protein composition), and pharmacologically (by differential sensitivity to AlF_4). By performing a kinetic analysis in polarized MDCK cells doubly transfected with recycling and transcytotic receptors, we have been also able to dissect functional differences between the two populations. This was possible since use of MDCK cells allowed us to directly measure two distinct recycling pathways, basolateral recycling versus transcytosis, and to monitor the effects of various manipulations on their kinetic properties. Based on the physical and functional distinctiveness of EEs and REs, it is now appropriate to refer to them as compartments, although such references have appeared previously without the minimal requirements for defining compartments having been met (Mellman and Simons, 1992).

EE and RE have distinct protein compositions as indicated by the observations that TfnR and rab11 are found preferentially with REs while rab4 is found preferentially with EEs, by both Western blot and immunocytochemistry on the isolated fractions. Given the obvious pathway relationship between EEs and REs, however, it is expected that the distributions of any given markers between the two compartments will be less than complete.

Our results also illustrate the distinct functions of EEs and REs, evidenced by both the distribution of TfnR and kinetic analysis of the transit of Tfn. At equilibrium, most of the internal TfnR is associated with the RE rather than the EE, despite the fact that EE appear to account for the large majority of recycling back to the basolateral surface. Based on the model, it appears that EE return >65% of basolaterally recycling TfnR as well as a significant fraction of receptors targeted for transcytosis. EE-mediated recycling also appears to be rapid, being completed within 10 min of internalization. Thus, from first principles, it now seems likely that the rapid phase of Tfn recycling occurs directly from EEs, rather than via rapid transit through REs as presumed previously.

On the other hand, our model predicts that EEs have at best a minor role in sorting receptors to the apical surface. This activity appears to be the purview of REs. Although the model predicts that pIgR may be transferred from EEs to REs somewhat more efficiently than TfnR, sorting in

the REs of pIgR-bound dIgA from TfnR is virtually complete. The kinetic analysis revealed that few if any dIgA–pIgR complexes are likely to be transported directly from REs to the basolateral plasma membrane, although a fraction are returned in a retrograde fashion to EEs (from which basolateral recycling presumably could once again occur). In contrast, very little of the Tfn that reaches RE is transferred to the apical surface, most of it being sorted basolaterally. It is precisely this sorting event that appears to be blocked by AlF_4. By this view, then, the recycling pathway consists of two endosomal compartments which function in tandem to ensure the polarized recycling of receptors internalized from the basolateral surface.

Certainly, our conclusions are limited by the fact that many important points were derived from kinetic analysis. In enzymology, it is well known that kinetics can never be used to assign precise reaction mechanism but only can be consistent with predicted models. Nevertheless, as sometimes occurs in enzymology, kinetic analysis can be the best or only possible strategy. Despite our ability to resolve EE from RE on density gradients, the degree of separation was incomplete, making it difficult to precisely quantify the localization of Tfn or dIgA to one or the other endosome compartment, particularly at time points when both tracers would be variably present both in EE and RE. It is highly likely that precise measurements would be needed, since targeting on the endocytic pathway is characterized by iterative low efficiency sorting events as opposed to single sorting reactions that result in complete separations at each cycle (Mayor et al., 1993; Marsh et al., 1995; Mellman, 1996). Thus, we would anticipate that the relative concentrations of Tfn versus dIgA in EE or RE would not vary markedly, making direct determinations difficult even after separation methods are improved.

Mathematical methods have been used in the past to describe recycling of Tfn and other ligands in a variety of cell lines. Although there have been some suggestions that multiple routes for recycling from the endosomes to the basolateral membrane may exist (O'Keefe and Draper, 1988; Gruenberg and Maxfield, 1995), most of these models assumed obligatory passage of ligand through the REs or rationalized the slower component of recycling in terms of nonvectoral retrograde flow between the two compartments (Wiley and Cunningham, 1982; Ciechanover et al., 1983; Hopkins and Trowbridge, 1983; Owensby et al., 1989; Ghosh et al., 1994; Lauffenburger and French, 1996; French and Lauffenburger, 1997). Our analysis has as its foundation the biochemical separation of two distinct endosomal populations. Thus, our approach involved fitting a series of accurate measurements for internalization and recycling into the minimum number of compartments known to be involved, rather than using kinetic modeling to predict the existence of the compartments themselves. This is a crucial point.

Our model was defined by a series of first order rate constants that describe only the transfer rate of ligand from one compartment to another, without making any assumptions concerning the nature of the compartments. Curve fitting was performed by systematically varying each of the rate constants that must interconnect EEs with REs, as well as both compartments with the plasma membrane. By constraining the progress curves by four experimental measurements in each case (rates of surface clearance, endocytosis, basolateral recycling, transcytosis), unique calculated solutions could be obtained for each data set. Best fits were stringently evaluated, first by eye, then by minimizing the sum squared errors (a common regression fitting technique). Comparative fits of different models were then performed using the well characterized statistical method of the Fischer F-test using a table of F values and degrees of freedom to provide the *P* value for relative significance of the fit improvement between models.

Our interpretation that the majority of basolateral to apical transcytosis reflects a sorting event in RE is consistent with recent results showing that rab17 is enriched in perinuclear RE structures in mouse mammary epithelial cells and that disruption of rab17 function by the expression of a dominant negative rab17 cDNA inhibits transcytosis but not basolateral recycling (Hunziker and Peters, 1998; Lutcke et al., 1993; Zacchi et al., 1998).

Other Mathematical Models

There are, a priori, many mathematical constructs which could be designed to model our recycling and transcytosis data. However, any model must reflect not only the kinetic data for recycling and transcytosis of Tfn and dIgA, but also for the passage through distinct endosomal populations. It is instructive to consider several such alternatives. For example, as discussed above, a model invoking a single pathway for Tfn passing obligatorily through the EEs and REs before recycling cannot be made to fit the experimental data and thus can be ruled out. To date, this has been the most widely presumed model for Tfn recycling, certainly in nonpolarized cells (Gruenberg and Maxfield, 1995). Similarly, models invoking a single endosomal compartment (Fig. 11 A, column 1) can be ruled out because they do not accurately fit the data for AlF_4-treated cells (Fig. 11 A, column 2), nor do they match the data demonstrating that Tfn passes through distinct compartments (Fig. 11 A, column 3).

Similarly, a model invoking two compartments with entirely distinct functions in basolateral recycling and apical transcytosis (Fig. 11 B) can be evaluated and eliminated. In this case, there is not direct passage from the RE to the basolateral surface, and AlF_4 might affect the retrograde RE to EE transport or partially affect transport from EE to the basolateral surface. Such a model can be nicely made to fit the experimentally derived kinetic data (Fig. 11 B, column 2). However, it makes the prediction that the EE will contain as much or more Tfn than the RE in untreated cells even at 20 min (Fig. 11 B, column 3). This prediction is not consistent with either the fluorescence or density gradient fractionation data.

While a minimum of two compartments and two recycling pathways must exist (based on kinetics and cell fractionation), it is theoretically possible to add compartments between the plasma membrane and the EE or RE and still fit the experimental data. For example a compartment can be added between the basolateral membrane and the EE (Fig. 11 C, column 1) and the experimental data will still fit well (Fig. 11 C, column 2). Also, the predictions for Tfn transport through EEs and REs Tfn content will be unal-

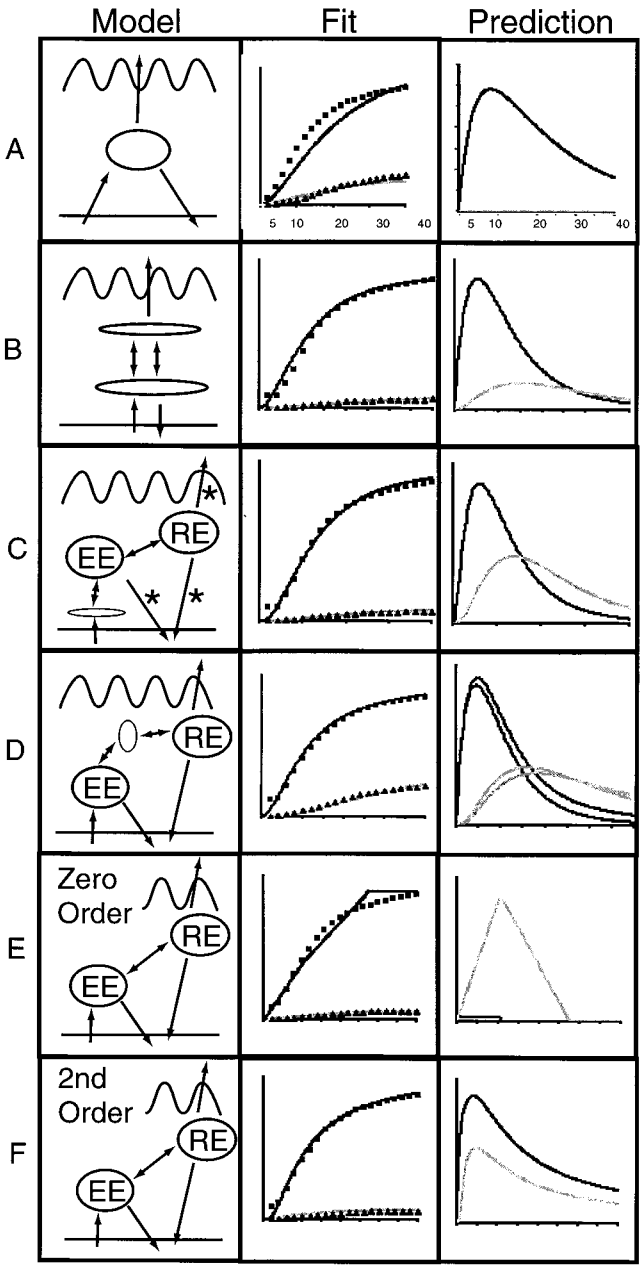

Figure 11. Alternative mathematical models are not all equal. Alternative mathematical models were constructed to describe endosomal processing of Tfn. Representative alternatives are illustrated in column 1 (Model). To be acceptable they must fit the experimental kinetic data (column 2, Fit) and make accurate predictions about the passage of Tfn through EEs and REs. For each model, the predicted curves for Tfn localization in EE and RE at various time points are shown in column 3 (Prediction). For all fit graphs, squares are recycling data, triangles are transcytosis data, black line is modeled recycling, and gray line is modeled transcytosis; y-axis is 0–100% of initially bound Tfn, x-axis is 0–40 min. For all prediction graphs, black line is EE and gray line is RE; y-axis is 0–40% of initially bound Tfn, x-axis is 0–40 min. (A) A single compartment model in the presence of AlF_4 fails to fit the recycling data (column 2, Fit) or to account for the observed passage of Tfn through the two physically distinct endosome populations. (B) A dual compartment model in which there is no direct pathway from the RE to the basolateral surface incorrectly predicts that the amount of Tfn in the EE will be greater than or equal to that in the RE in untreated cells even at 25 min after internalization (see column 3, Prediction). (C) Addition of a compartment between the basolateral membrane and the EE still fits the kinetic data and makes an acceptable prediction about internal localization as long as the rate of surface clearance into the new compartment is 0.21 (equal to the calculated rate from basolateral membrane to EE in our model) and the rate out of the new compartment to the EE is >1. Additional compartments may also be placed at asterisks with similar results (not shown). (D) Addition of a compartment between EEs and REs under AlF_4 conditions fits kinetic experimental data but incorrectly predicts little change in the amount of Tfn in RE after addition of AlF_4. In the prediction column, the two black lines indicate Tfn in EE, and the two gray lines indicate Tfn in RE. The upper line at 20 min in each pair represents the AlF_4-treated cells. (E) A two-compartment, two-pathway model as described in Fig. 6 C but using zero order rate constants fails to match the form of the progress curves generated experimentally. (F) A two-compartment, two-pathway model as described in Fig. 6 C but using second order rate constants fits the experimentally derived data, but incorrectly predicts that for untreated cells, the level of Tfn in EE will always exceed that in REs.

tered (Fig. 11 C, column 3). However, the rate of exit from the newly added compartment must be close to 1.2 min^{-1}, severalfold more rapid even than the initial internalization step and not consistent with values derived from morphologic analysis (Ghosh and Maxfield, 1995). Additional compartments can be added along the exit pathways from EEs and REs to the plasma membrane (Fig. 11 C, column 1, asterisks) only so long as the rate of exit from the EE or RE is not altered and the rate of exit from the added compartment exceeds the rate of entry into that compartment.

As with the addition of compartments between EEs, REs, or the plasma membrane, addition of a compartment between EEs and REs cannot be ruled out (Fig. 11 D). This model can be adapted to fit the experimental kinetic Tfn recycling data in control cells (not shown) and in AlF_4-treated cells (Fig. 11 D, column 2). However, it predicts that addition of AlF_4 will result in an accumulation of one-third of the intracellular Tfn at 20 min into the new compartment, while the total amount in EEs and REs will remain unaffected (Fig. 11 D, column 3). Microscopy failed to detect a third morphologically distinct compartment, and no third peak was detected by subcellular fractionation. However, these techniques might miss a compartment with similar morphology and density characteristics to the RE. Thus, while the presence of a compartment between EEs and REs is unlikely, it cannot be ruled out.

Finally, we have made the assumption that the kinetics describing transport between compartments are first order, where the generalized equation is $d[A]/dt = -k[A]$, where $[A]$ is the concentration of Tfn (or TfnR) in a given compartment and k is the rate constant (see Materials and Methods). Since all of the Tfn is bound to TfnR and under the assay conditions essentially all of the TfnR is occupied by either labeled or unlabeled Tfn, the movement of Tfn–TfnR complexes will be a pseudo first order process. Since these assumptions may not be true, the same model can be constructed using zero order kinetic rates such that $d[A]/dt = -(k$ or $[A]$, whichever is lesser). The progress curves

produced by such a model are clearly different than the experimentally derived data (Fig. 11 E, column 2). Furthermore, a two-compartment, two-pathway zero order model predicts that virtually all of the internalized Tfn will be in the RE even at short times of internalization (2.5 min), clearly at odds with the fluorescence and cell fractionation data. Alternatively, a second order process can be envisioned where both the concentration of Tfn and its receptor play a role such that $d[TfnR]/dt = -k[Tfn][TfnR]$. However, since the receptor is essentially fully occupied by the ligand, such a process will reduce a pseudo first order kinetics where $d[Tfn - TfnR]/dt = -k[Tfn - TfnR]$. Still, it is possible there exists some level of cooperativity among the receptors so that the process would still exhibit a second order response to receptor concentration, such that $d[Tfn]/dt = -k[Tfn]^2$. A model based on second order equations (Fig. 11 F) can be made to fit the experimental data (Fig. 11 F, column 2). However, the model predicts that in untreated cells, EEs will always contain more Tfn than REs, which is clearly not the case.

Signals, Kinetics, and Polarized Sorting in Endosomes

In epithelial cells, the polarity of receptors and other membrane proteins is determined by a hierarchical arrangement of sorting signals that ensure proper basolateral or apical targeting (Matter and Mellman, 1994). Similar or identical signals are decoded in endosomes and the trans-Golgi network. Since receptors such as TfnR are retained almost entirely at the basolateral surface, it must therefore be presumed that recycling is a signal-directed, nonrandom process. However, at least in nonpolarized cells, the apparent rate of TfnR recycling appears indistinguishable from that of bulk membrane lipid, data which have been interpreted to mean that recycling occurs by default (Matlin, 1992; Mayor et al., 1993).

The finding that EEs and REs have distinct sorting features suggests an attractive way to reconcile these apparently disparate ideas. Most recycling from EEs in MDCK cells appears to be directed towards the basolateral surface, and the fidelity of recycling is not affected by AlF_4. Conceivably, then, there is a nonselective bulk flow of membrane from EEs to the basolateral plasma membrane that might result in the rapid, and possibly even signal-independent, transfer of receptors (TfnR, pIgR) and lipids back to their surface of origin. Those receptors that are transferred to RE, however, may be subjected to a signal-dependent sorting event. Thus, TfnR would be efficiently sorted from pIgR, whose basolateral targeting signal may be inactivated as a result of having bound dIgA (Casanova et al., 1990; Song et al., 1994). This sorting event presumably reflects the sequestration of TfnR into transport vesicles destined for the basolateral surface while pIgR would be sequestered into apically directed vesicles. AlF_4 may act to prevent the REs from sequestering receptors into such basolateral recycling vesicles. While this information does not bring us much closer to understanding the molecular mechanism of polarized sorting, it does give an important and long awaited hint regarding where to look.

Received for publication 24 March 1998 and in revised form 23 February 1999.

References

Advani, R.J., H.R. Bae, J.B. Bock, D.S. Chao, Y.C. Doung, R. Prekeris, J.S. Yoo, and R.H. Scheller. 1998. Seven novel mammalian SNARE proteins localize to distinct membrane compartments. *J. Biol. Chem.* 273:10317–10324.

Apodaca, G., L.A. Katz, and K.E. Mostov. 1994. Receptor-mediated transcytosis of IgA in MDCK cells is via apical recycling endosomes. *J. Cell Biol.* 125: 67–86.

Barroso, M., and E.S. Sztul. 1994. Basolateral to apical transcytosis in polarized cells is indirect and involves BFA and trimeric G protein sensitive passage through the apical endosome. *J. Cell Biol.* 124:83–100.

Besterman, J.M., J.A. Airhart, R.C. Woodworth, and R.B. Low. 1981. Exocytosis and pinocytosed fluid in cultured cells: kinetic evidence for rapid turnover and compartmentation. *J. Cell Biol.* 91:716–727.

Breitfeld, P.P., J.M. Harris, and K.E. Mostov. 1989. Postendocytotic sorting of the ligand for the polymeric immunoglobulin receptor in Madin-Darby canine kidney cells. *J. Cell Biol.* 109:475–486.

Breitfeld, P.P., J.E. Casanova, W.C. McKinnon, and K.E. Mostov. 1990. Deletions in the cytoplasmic domain of the polymeric immunoglobulin receptor differentially affect endocytotic rate and postendocytotic traffic. *J. Biol. Chem.* 265:13750–13757.

Casanova, J.E., P.P. Breitfeld, S.A. Ross, and K.E. Mostov. 1990. Phosphorylation of the polymeric immunoglobulin receptor required for its efficient transcytosis. *Science.* 248:742–745.

Ciechanover, A., A.L. Schwartz, A. Cautry-Varsat, and H.F. Lodish. 1983. Kinetics of internalization of transferrin and the transferrin receptor in a human hepatoma cell line. *J. Biol. Chem.* 258:9681–9689.

Daniel, W.W. 1987. Biostatistics: A Foundation for Analysis in the Health Sciences. John Wiley & Sons, New York. 127–187.

Daro, E., P. Van der Sluijs, T. Galli, and I. Mellman. 1996. Rab4 and cellubrevin define different early endosome populations on the pathway of transferrin receptor recycling. *Proc. Natl. Acad. Sci. USA.* 93:9559–9564.

French, A.R., and D.A. Lauffenburger. 1997. Controlling receptor/ligand trafficking: effects of cellular and molecular properties on endosomal sorting. *Ann. Biomed. Eng.* 25:690–707.

Futter, C.E., A. Gibson, E.H. Allchin, S. Maxwell, L.J. Ruddock, G. Odorizzi, D. Domingo, I.S. Trowbridge, and C.R. Hopkins. 1998. In polarized MDCK cells basolateral vesicles arise from clathrin-γ-adaptin-coated domains on endosomal tubules. *J. Cell Biol.* 141:611–623.

Ghosh, R.N., and F.R. Maxfield. 1995. Evidence for nonvectorial, retrograde transferrin traffic in the early endosomes of Hep2 cells. *J. Cell Biol.* 128:549–561.

Ghosh, R.N., D.L. Gelman, and F.R. Maxfield. 1994. Quantification of low density lipoprotein and transferrin endocytic sorting in Hep2 cells using confocal microscopy. *J. Cell Sci.* 107:2177–2189.

Gibson, A., C.E. Futter, S. Maxwell, E.H. Allchin, M. Shipman, J. Kraehenbuhl, D. Domingo, G. Odorizzi, I.S. Trowbridge, and C.R. Hopkins. 1998. Sorting mechanisms regulating membrane protein traffic in the apical transcytotic pathway of polarized MDCK cells. *J. Cell Biol.* 143:81–94.

Green, S.A., K.P. Zimmer, G. Griffiths, and I. Mellman. 1987. Kinetics of intracellular transport and sorting of lysosomal membrane and plasma membrane proteins. *J. Cell Biol.* 105:1227–1240.

Gruenberg, J., and F.R. Maxfield. 1995. Membrane transport in the endocytic pathway. *Curr. Opin. Cell Biol.* 7:552–563.

Hopkins, C.R. 1994. Internalization of polypeptide growth factor receptors and the regulation of transcription. *Biochem. Pharmacol.* 47:151–154.

Hopkins, C.R., and I.S. Trowbridge. 1983. Internalization and processing of transferrin and the transferrin receptor in human carcinoma A431 cells. *J. Cell Biol.* 97:508–521.

Hunziker, W., and P.J. Peters. 1998. Rab17 localizes to recycling endosomes and regulates receptor-mediated transcytosis in epithelial cells. *J. Biol. Chem.* 273:15734–15741.

Hunziker, W., J.A. Whitney, and I. Mellman. 1991. Selective inhibition of transcytosis by Brefeldin A in MDCK cells. *Cell.* 67:617–627.

Lai, A., A. Gibson, C.R. Hopkins, and I.S. Trowbridge. 1998. Signal-dependent trafficking of beta-amyloid precursor protein-transferrin receptor chimeras in Madin-Darby canine kidney cells. *J. Biol. Chem.* 273:3732–3739.

Lauffenburger, D.A., and A.R. French. 1996. Intracellular receptor/ligand sorting based on endosomal retenton components. *Biotechnol. Bioeng.* 51:281–297.

Lutcke, A., S. Jansson, R.G. Parton, P. Chavrier, A. Valencia, L.A. Huber, E. Lehtonen, and M. Zerial. 1993. Rab17, a novel small GTPase, is specific for epithelial cells and is induced during cell polarization. *J. Cell Biol.* 121:553–564.

Marsh, E.W., P.L. Loepold, N.L. Jones, and F.R. Maxfield. 1995. Oligomerized transferrin receptors are selectively retained by a lumenal sorting signal in a long-lived endocytic recycling compartment. *J. Cell Biol.* 129:1509–1522.

Matlin, K.S. 1992. W(h)ither default? Sorting and polarization in epithelial cells. *Curr. Opin. Cell Biol.* 4:623–628.

Matter, K., and I. Mellman. 1994. Mechanisms of cell polarity: sorting and transport in epithelial cells. *Curr. Opin. Cell Biol.* 6:545–554.

Matter, K., W. Hunziker, and I. Mellman. 1992. Basolateral sorting of LDL receptor in MDCK cells: the cytoplasmic domain contains two tyrosine dependent targeting determinants. *Cell.* 71:1–20.

Matter, K., J.A. Whitney, E. Miller, and I. Mellman. 1993. Common signals control LDL receptor sorting in endosomes and the Golgi of MDCK cells. *Cell.* 74:1053–1064.

Mayor, S., J.F. Presley, and F.R. Maxfield. 1993. Sorting of membrane compo-

nents from endosomes and subsequent recycling to the cell surface occurs by a bulk flow process. *J. Cell Biol.* 121:1257–1269.

Mellman, I. 1996. Endocytosis and molecular sorting. *Ann. Rev. Cell Dev. Biol.* 12:575–625.

Mellman, I., and K. Simons. 1992. The Golgi complex: in vitro veritas? *Cell.* 68: 829–840.

Mostov, K.E. 1995. Regulation of protein traffic in polarized epithelial cells. *Histol. Histopathol.* 10:423–431.

Mostov, K.E., M. Friedlander, and G. Blobel. 1984. The receptor for transepithelial transport of IgA and IgM contains multiple immunoglobulin-like domains. *Nature.* 308:37–43.

Motulsky, H.J., and L.A. Ransnas. 1987. Fitting curves to data using nonlinear regression: a practical and nonmathematical review. *FASEB (Fed. Am. Soc. Exp. Biol.) J.* 1:365–374.

Odorizzi, G., A. Pearse, D. Domingo, I.S. Trowbridge, and C.R. Hopkins. 1996. Apical and basolateral endosomes of MDCK cells are interconnected and contain a polarized sorting mechanism. *J. Cell Biol.* 135:139–152.

O'Keefe, D.O., and R.L. Draper. 1988. Two pathways of transferrin recycling evident in a variant of mouse LMTK$^-$ cells. *Som. Cell Mol. Genet.* 14:473–487.

Owensby, D.A., P.A. Morton, and A.L. Schwartz. 1989. Quantitative evaluation of receptor-mediated endocytosis. *Methods Cell Biol.* 32:305–327.

Podbilewicz, B., and I. Mellman. 1990. ATP and cytosol requirements for transferrin recycling in intact and disrupted MDCK cells. *EMBO (Eur. Mol. Biol. Organ.) J.* 9:3477–3487.

Presley, J.F., S. Mayor, K.W. Dunn, L.S. Johnson, T.E. McGraw, and F.R. Maxfield. 1993. The End2 mutation in CHO cells slows the exit of transferrin receptors from the recycling compartment but bulk membrane recycling if unaffected. *J. Cell Biol.* 122:1231–1241.

Schaerer, E., F. Verrey, L. Racine, C. Tallichet, M. Reinhardt, and J.P. Kraehenbuhl. 1990. Polarized transport of the polymeric immunoglobulin receptor in transfected rabbit mammary epithelial cells. *J. Cell Biol.* 110:987–998.

Schmid, S.L., R. Fuchs, P. Male, and I. Mellman. 1988. Two distinct subpopulations of endosomes involved in membrane recycling and transport to lysosomes. *Cell.* 52:73–83.

Simons, K., and E. Ikonen. 1997. Functional rafts in cell membranes. *Nature.* 387:569–572.

Song, W., G. Apodaca, and K. Mostov. 1994. Transcytosis of the polymeric immunoglobulin receptor is regulated in multiple intracellular compartments. *J. Biol. Chem.* 269:29474–29480.

Sternweis, P.C., and A.G. Gilman. 1982. Aluminum: a requirement for activation of the regulatory component of adenylate cyclase by fluoride. *Proc. Natl. Acad. Sci. USA.* 79:4888–4891.

Trowbridge, I.S., R.A. Newman, D.L. Domingo, and C. Sauvage. 1984. Transferrin receptors: structure and function. *Biochem. Pharmacol.* 33:925–932.

Ullrich, O., S. Reinsch, S. Urbe, M. Zerial, and R.G. Parton. 1996. Rab11 regulates recycling through the pericentriolar recycling endosome. *J. Cell Biol.* 135:913–924.

Wiley, H.S., and D.D. Cunningham. 1982. The endocytic rate constant. *J. Biol. Chem.* 257:4222–4229.

Yamashiro, D.J., B. Tycko, S.R. Fluss, and F.R. Maxfield. 1984. Segregation of transferrin to a mildly acidic (pH 6.5) para-Golgi compartment in the recycling pathway. *Cell.* 37:789–800.

Zacchi, P., H. Stenmark, R.G. Parton, D. Orioli, F. Lim, A. Giner, I. Mellman, M. Zerial, and C. Murphy. 1998. Rab17 regulates membrane trafficking through apical recycling endosomes in polarized epithelial cells. *J. Cell Biol.* 140:1039–1053.